Dressing effects in the laser-assisted (e, $2e$) process in fast-electron–hydrogen-atom collisions in an asymmetric coplanar scattering geometry

Gabriela Buică*
Institute of Space Science, P.O. Box MG-36, 77125, Bucharest-Măgurele, Romania

(Received 14 February 2022; accepted 26 July 2022; published 10 August 2022)

We present the theoretical treatment of laser-assisted (e, $2e$) ionizing collisions in hydrogen for fast electrons, in the framework of the first-order Born approximation at moderate laser intensities and photon energies beyond the soft-photon approximation. The interaction of the laser field with the incident, scattered, and ejected electrons is treated nonperturbatively by using Gordon-Volkov wave functions, while the atomic dressing is treated by using first-order perturbation theory. Within this semiperturbative formalism, we obtain a closed-form formula for the nonlinear triple differential cross section (TDCS), which is valid for linear as well circular polarizations. Analytical simple expressions of TDCS are derived in the weak field domain and low-photon energy limit. It was found that for nonresonant (e, $2e$) reactions, the analytical formulas obtained for the atomic matrix element in the low-photon energy limit give a good agreement, qualitative and quantitative, with the numerical semiperturbative model calculations. We study the influence of the photon energy as well of the kinetic energy of the ejected electron on the TDCS, in the asymmetric coplanar geometry, and show that the dressing of the atomic target strongly influences the (e, $2e$) ionization process. We discuss the exchange effects between the ejected and scattered electrons in the TDCS.

DOI: 10.1103/PhysRevA.106.022804

I. INTRODUCTION

It is well known that the study of the atomic ionization process by collisions with electrons, the so-called (e, $2e$) reaction, reveals information about the electronic structure of the atomic target and residual ion [1], and is of interest in collision theory or in other fields such as plasma physics or astrophysics, which need reliable scattering cross-section data [2]. Camilloni and coworkers [3] were the first to use (e, $2e$) reaction as a tool for measuring the momentum distribution of the ejected electrons, in a coplanar symmetric scattering geometry where the outgoing electrons have equal energies and polar angles, at high incident and outgoing electron energies. Since then, an increasing number of (e, $2e$) experiments have been performed over the years for different target atoms and for various kinematical configurations, and the electron momentum spectroscopy (EMS) has been developed to provide information on the electronic structure of atoms and molecules [4,5]. The symmetric (e, $2e$) reaction is the basis of EMS, also known as binary (e, $2e$) spectroscopy, and is kinematically characterized by a large momentum transfer of the projectile electron and a small momentum of the residual ion. Another useful scattering configuration is the coplanar asymmetric geometry with fast incident electrons (keV) and ejected electrons of low and moderate energies, where most of the (e, $2e$) reactions occur [6].

In the past few decades, the electron-impact ionization of an atom in the presence of a laser field has become increasingly interesting and it is often referred to as the *laser-assisted* (e, $2e$) *collision* [7]. Recently, Höhr and coworkers [8] performed the first kinematically complete experiment for laser-assisted ionization in electron-helium collisions at high incident electron energy (1 keV) and showed significant differences of the triple differential cross section (TDCS) in comparison to the field-free cross sections. Very recently, Hiroi and coworkers [9] reported the observation the laser-assisted electron-impact ionization of Ar in an ultrashort intense laser field and showed that the signal intensity of the laser-assisted process for one-photon absorption obtained by integrating the signals over the detection angle ranges is about twice as large as that estimated by previous theoretical calculations in which the atomic dressing by the laser field is neglected [10].

A large number of papers have been published so far and several theoretical approaches have been proposed, involving ejected electrons of low energies that are studied under the combined influence of the laser field and the Coulomb field of the residual ion. The early theoretical works on laser-assisted (e, $2e$) scattering have neglected the dressing of the atomic target by the laser field or have used the closure approximation for laser-atom interaction. First, Jain and Tzoar introduced the Coulomb-Volkov wave functions [11], which takes into account the influence of the Coulomb field of the nucleus on the final electron state. Since then, the effect of the Coulomb interaction in the laser-assisted (e, $2e$) collisions on hydrogen atoms was studied in several papers by employing different types of final-state wave functions like the Coulomb-Volkov or Coulomb-corrected Gordon-Volkov wave functions. Banerji and Mittleman [12] calculated TDCS for ionization of hydrogen by electron impact, at low photon energies, in which the slow ejected electron was described by

*buica@spacescience.ro

a modified Coulomb wave function, and the laser-electrons interactions were included in the low-frequency approximation. Cavaliere and coworkers [10] studied laser-assisted $(e, 2e)$ collisions in hydrogen at low photon energies, high incident electron energies, and ejected electrons with moderate as well as small energies, in the first-order Born approximation, with the incident and scattered electrons described by the Gordon-Volkov wave functions [13,14], while the ejected electron was represented by a modified Coulomb wave function. Later on, the dressing of the atomic target by the laser field has been included in the first-order time-dependent perturbation theory (TDPT), and therefore the influence of the laser parameters such as intensity, polarization, and photon energy has attracted a lot of interest from the theoretical point of view. Joachain and coworkers [15] extended the semiperturbative theory of Byron and Joachain [16] and showed the strong influence of a laser field on the dynamics of laser-assisted $(e, 2e)$ collisions in hydrogen, for fast incident and scattered electrons and slow ejected electrons, in the Ehrhardt asymmetric coplanar geometry [17]. For $(e, 2e)$ collisions in hydrogen with slow ejected electrons, Martin and coworkers [18] analyzed the influence of the laser parameters: photon energy, laser intensity, and polarization direction on the angular distribution of the ejected electrons. The influence of laser polarization has also been discussed by Taïeb and coworkers [19], who developed a dressed atomic wave functions on a basis of Sturmian functions, which allowed to take into account accurately the contribution of the continuum spectrum to the dressing of the atomic states [20]. Very recently, Makhoute and coworkers [21] presented their numerical results obtained for $(e, 2e)$ collision in atomic hydrogen in the symmetric and asymmetric coplanar scattering geometries, at large photon energies. For the direct scattering channel, the calculation of the specific radial amplitudes was performed by expanding the atomic wave functions in a Sturmian basis, whereas the closure approximation was employed for the exchange channel.

As mentioned before, most of these previous theoretical works were focused on scattering geometries involving slow ejected electrons, and only recently it was shown for ejected electrons of high energies that the laser field strongly modifies the $(e, 2e)$ collisions. New theoretical studies for laser-assisted EMS at high impact energy and large momentum transfer were published and it was found that the atomic dressing, calculated in the closure- and low-frequency approximations, substantially influences the laser-assisted TDCSs at low [22,23] and large photon energies [24].

The purpose of the present paper is to study the laser-assisted $(e, 2e)$ reactions in hydrogen, in which the target atom is ionized in collision with an electron beam in the presence of a laser field, for fast incident and outgoing electrons, in an asymmetric coplanar scattering geometry, beyond the soft-photon approximation. We present a method to derive the relevant atomic transition amplitude which takes into account the dressing of the target by the laser field. The laser field alone cannot significantly ionize the hydrogen atom since the photon energy is considered below the ionization threshold and the laser intensity is not high enough to allow ionization through a multiphoton process. We assume fast scattered electrons of sufficiently high velocity, such that we neglect their interaction with the Coulomb field of the remaining ion. Similar to the approach used in the Keldysh-Faisal-Reiss approximation [25–27], the influence of the remaining ion on the final state of the fast ejected electron is neglected, since the residual Coulomb field is weak compared to the laser field strength. We follow the approach of Ref. [15] in which the semiperturbative theory [16] was generalized to laser-assisted fast $(e, 2e)$ collisions in atomic hydrogen. In order to simplify the calculations, we introduce several assumptions: (a) It is reasonable to employ a first-order Born treatment of the projectile-atom interaction, since we consider fast nonrelativistic collisions such that the velocities of the projectile and outgoing electrons are much larger than the atomic unit [28,29]. (b) The nonrelativistic Gordon-Volkov solutions are used for the incident and outgoing electrons to describe their interaction with the laser field. (c) The laser field intensity is considered moderate, but much weaker than the atomic unit ($3.51 \times 10^{16}\,\mathrm{W/cm^2}$), in order to avoid direct one- and multiphoton ionization. In contrast to other theoretical works, we take into account the atomic dressing effects in the first-order TDPT in the laser field, going beyond the soft-photon approximation. The photon energy is considered below the ionization threshold of the hydrogen atom, and one-photon resonance transitions are allowed between the ground and excited states. (d) Since the scattered and ejected electrons may have high kinetic energies of comparable order of magnitude, our semiperturbative formalism takes into account the exchange effects in the first-order Born approximation.

The paper is organized as follows. In Sec. II, we present the theoretical method used in laser-assisted ionization of atomic hydrogen by electron impact, and derive analytical formulas for the ionization transition amplitudes and TDCSs by electron impact. In the low-photon energy limit, we provide simple analytic formulas of TDCSs, in a closed form, for the laser-assisted $(e, 2e)$ ionization process which include the atomic dressing effects. Numerical results are presented in Sec. III, where the TDCSs for laser-assisted electron impact ionization of hydrogen are analyzed as a function of the scattering angle of the ejected electron and as a function of the photon energy. We study the modifications of the angular distributions of the ejected electrons due to the external laser field at different ejected electron energies and photon energies. We discuss the exchange effects between the ejected and scattered electrons by comparing the direct and exchange contributions to TDCS. Finally, summary and conclusions are given in Sec. IV. Atomic units (a.u.) are employed throughout this paper, unless otherwise specified.

II. SEMIPERTURBATIVE THEORY

The laser-assisted scattering of electrons by hydrogen atoms in a laser field in which the atomic target is ionized, the so-called laser-assisted $(e, 2e)$ reaction, can be symbolically represented as

$$e^-(E_i, \mathbf{k}_i) + \mathrm{H}(1s) + N_i\,\gamma(\omega, \boldsymbol{\varepsilon}) \rightarrow e^-(E_f, \mathbf{k}_f) + e^-(E_e, \mathbf{k}_e) + \mathrm{H}^+ + N_f\,\gamma(\omega, \boldsymbol{\varepsilon}), \quad (1)$$

where E_i and E_f, and $\mathbf{k}_i\,(\theta_i, \varphi_i)$ and $\mathbf{k}_f\,(\theta_f, \varphi_f)$, represent the kinetic energy and the momentum vector of the incident and scattered projectile electrons, respectively, while E_e and

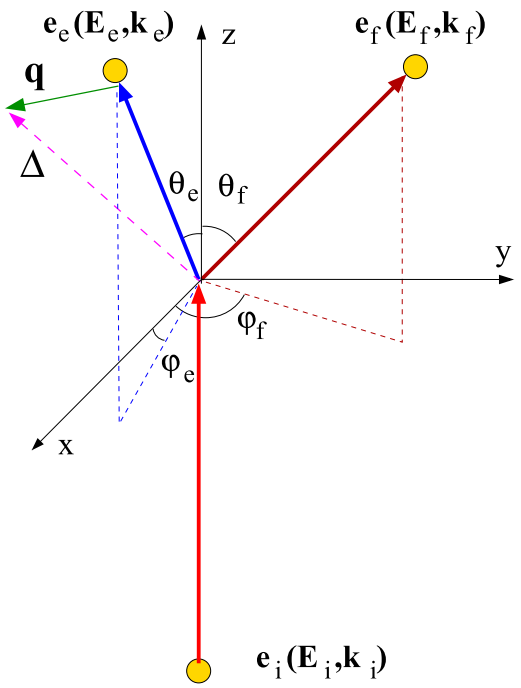

FIG. 1. Schematic representation of the scattering geometry for the $(e, 2e)$ reaction. The incident electron has energy E_i and momentum $\mathbf{k_i}$, while the scattered electron has energy E_f and momentum $\mathbf{k_f}$, and is detected at a fixed scattering angle θ_f. The ejected electron has energy E_e and momentum $\mathbf{k_e}$, and its detection angle θ_e is varied. $\mathbf{\Delta} = \mathbf{k_i} - \mathbf{k_f}$ denotes the momentum transfer vector from the incident to the scattered electron, and $\mathbf{q} = \mathbf{\Delta} - \mathbf{k_e}$ is ion recoil momentum vector. For a coplanar scattering geometry lying in the (x, z) plane the azimuthal angles φ_f and φ_e are equal to 0° or 180°, with the incident electron propagating in the z-axis direction, $\varphi_i = 0^\circ$ and $\theta_i = 0^\circ$.

$\mathbf{k}_e\,(\theta_e, \varphi_e)$ are the kinetic energy and the momentum vector of the ejected electron, as plotted in Fig. 1. Here $\gamma\ (\omega, \boldsymbol{\varepsilon})$ denotes a photon with the energy ω and the unit polarization vector $\boldsymbol{\varepsilon}$, and $N = N_i - N_f$ is the net number of exchanged photons between the projectile-atom scattering system and the laser field.

The laser field is treated classically, and within the dipole approximation is described as a monochromatic electric field,

$$\boldsymbol{\mathcal{E}}(t) = (i/2)\,\mathcal{E}_0\,e^{-i\omega t}\,\boldsymbol{\varepsilon} + \text{c.c.}, \tag{2}$$

where $\mathcal{E}_0$ represents the amplitude of the electric field. The magnetic vector potential, $\boldsymbol{A}(t)$, is simply calculated from $\boldsymbol{\mathcal{E}}(t) = -\partial_t \boldsymbol{A}(t)$, as

$$\boldsymbol{A}(t) = (\mathcal{E}_0/\omega)[\cos\omega t\,\cos(\xi/2)\,\mathbf{e}_j + \sin\omega t\,\sin(\xi/2)\,\mathbf{e}_l], \tag{3}$$

where $\boldsymbol{\varepsilon} = \cos(\xi/2)\,\mathbf{e}_j + i\sin(\xi/2)\,\mathbf{e}_l$ is the polarization vector of the laser beam, with $\mathbf{e}_j$ and $\mathbf{e}_l$ being two different unit vectors along different orthogonal directions. ξ represents the degree of ellipticity of the laser field which varies in the range $-\pi/2 \leqslant \xi \leqslant \pi/2$ and determines the ellipticity of the field. The value $\xi = 0$ corresponds to a linearly polarized (LP) laser field, while $\xi = \pi/2$ corresponds to a left-hand circularly polarized (CP) laser field.

A. Laser-dressed electronic and atomic wave functions

As mentioned before, we consider that the external laser field has a dominant influence and neglect the Coulomb interaction between fast outgoing electrons and residual ion in the scattered and ejected electron wave functions [25–27]. At sufficiently high projectile kinetic energies, it is well known that the first-order Born approximation in the scattering potential can be used to describe the electron impact ionization process [15,28,29]. We assume fast incident and outgoing electrons with kinetic energies much larger than the energy of a bound electron in the first Bohr orbit [7], since for the field-free $(e, 2e)$ reaction in e-H collisions it is well known that the plane-wave approximations agree well with experiment at kinetic energies above 200 eV [28,30]. Thus, in the nonrelativistic regime, as long as both $E_f \gg 1$ a.u. and $E_e \gg 1$ a.u., we describe the fast scattered and ejected electrons by Gordon-Volkov wave functions [11,31,32]. We should mention that the use of a Coulomb-Volkov wave function provides a more accurate treatment at small impact kinetic energies, where the effect of the proton's potential on the incoming and outgoing electrons is important [2,7,33]. In order to avoid the direct one- and multiphoton ionization processes, we consider that the electric field amplitude is weak with respect to the atomic unit of electric field strengths, $\mathcal{E}_0 \ll 5.1 \times 10^9$ V/cm, i.e., the strength of the laser field is much lower than the Coulomb field strength experienced by an electron in the first Bohr orbit.

Therefore, we describe in a nonperturbative way the initial and final states of the projectile electron, as well the final state of the ejected electron interacting with a laser field by nonrelativistic Gordon-Volkov wave functions [13,14], expressed in the velocity gauge as

$$\chi^V_{\mathbf{k}}(\mathbf{r}, t) = (2\pi)^{-3/2} \exp\Big[i\mathbf{k}\cdot\mathbf{r} - i\mathbf{k}\cdot\boldsymbol{\alpha}(t) - iE_k\,t - \frac{i}{2}\int^t dt' \boldsymbol{A}^2(t')\Big], \tag{4}$$

where $\mathbf{r}$ and $\mathbf{k}$ represent the position and momentum vectors, and $E_k = k^2/2$ is the kinetic energy of the electron. $\boldsymbol{\alpha}(t) = \int^t dt' \boldsymbol{A}(t')$ describes the classical oscillation motion of a free electron in the electric field defined by Eq. (2), and by using Eq. (3) we obtain

$$\boldsymbol{\alpha}(t) = \alpha_0[\mathbf{e}_j \sin\omega t\,\cos(\xi/2) + \mathbf{e}_l \cos\omega t\,\sin(\xi/2)], \tag{5}$$

where $\alpha_0 = \sqrt{I}/\omega^2$ is the amplitude of oscillation, and $I = \mathcal{E}_0^2$ denotes the laser intensity. Obviously, as noticed from Eq. (4), at moderate field strengths the largest effect of the laser field on the free-electron state is determined by a dimensionless parameter $k\alpha_0$, which depends on the electron and photon energies, and laser intensity. For example, a laser intensity of 1 TW/cm^2, a photon energy of 3.1 eV, and an electron kinetic energy of 200 eV result in a value of $k\alpha_0 \simeq 1.58$, while the ponderomotive energy acquired by an electron in the electric field $U_p = I/4\omega^2$ is about 0.015 eV and therefore can be safely neglected compared to the photon and unbound electrons energies employed in the present paper.

The interaction of the hydrogen atom, initially in its ground state, with a laser field at moderate field strengths is considered within the first-order TDPT. An approximate solution for

the wave function of an electron bound to a Coulomb potential in the presence of an electric field, also known as the dressed wave function, is written as

$$\Psi_{1s}(\mathbf{r}_1,t)=\left[\psi_{1s}^{(0)}(\mathbf{r}_1,t)+\psi_{1s}^{(1)}(\mathbf{r}_1,t)\right]\times\exp\left[-iE_1t-\frac{i}{2}\int^t dt'\boldsymbol{A}^2(t')\right], \quad (6)$$

where $\mathbf{r}_1$ is the position vector of the bound electron, $\psi_{1s}^{(0)}$ is the unperturbed wave function of the hydrogen atom ground state, and $\psi_{1s}^{(1)}$ represents the first-order perturbative correction to the atomic wave function due to the external laser field. We employ the following expression of the first-order correction in the velocity gauge, $\psi_{1s}^{(1)}$, as described by Florescu and Marian in Ref. [34],

$$\psi_{1s}^{(1)}(\mathbf{r}_1,t)=-\frac{\alpha_0\omega}{2}\left[\boldsymbol{\varepsilon}\cdot\mathbf{w}_{100}\left(E_1^+;\mathbf{r}_1\right)e^{-i\omega t}+\boldsymbol{\varepsilon}^*\cdot\mathbf{w}_{100}\left(E_1^-;\mathbf{r}_1\right)e^{i\omega t}\right], \quad (7)$$

with the linear-response vector, $\mathbf{w}_{100}$, defined by

$$\mathbf{w}_{100}(E_1^{\pm};\mathbf{r}_1)=-G_C(E_1^{\pm})\,\mathbf{P}\,\psi_{1s}(\mathbf{r}_1), \quad (8)$$

where $\mathbf{P}$ denotes the momentum operator of the bound electron and G_C is the Coulomb Green's function. For the hydrogen atom in its ground state, the linear-response vector was expressed in Ref. [34] as

$$\mathbf{w}_{100}(E_1^{\pm};\mathbf{r}_1)=i(4\pi)^{-1/2}\mathcal{B}_{101}(E_1^{\pm};r_1)\,\hat{\mathbf{r}}_1, \quad (9)$$

where $\hat{\mathbf{r}}_1=\mathbf{r}_1/r_1$, and the energies E_1^+ and E_1^- take the following values,

$$E_1^+=E_1+\omega+i0,\quad E_1^-=E_1-\omega, \quad (10)$$

with $E_1=-13.6$ eV representing the energy of the ground state. The radial function $\mathcal{B}_{101}$ in Eq. (9) was evaluated [34] using the Schwinger's integral representation of the Coulomb Green's function in momentum space including both bound and continuum eigenstates, and can be expressed in terms of Humbert function, Φ_1, as

$$\mathcal{B}_{101}(\tau;r_1)=\frac{2\,\tau}{2-\tau}\left(\frac{2}{1+\tau}\right)^{2+\tau}r_1\,e^{-r_1/\tau}\times\Phi_1(2-\tau,-1-\tau,3-\tau,\xi_1,\eta_1), \quad (11)$$

where the parameter τ takes two values $\tau^{\pm}=1/\sqrt{-2E_1^{\pm}}$, and the variables of the Humbert function are $\xi_1=(1-\tau)/2$ and $\eta_1=(1-\tau)r_1/\tau$.

It is well known that differences between the length and velocity gauge calculations arise due to approximations utilized for particle–laser field interaction and accurate wave functions should be employed in order to have a good agreement of results obtained from different gauges [29]. In the past 30 years, the velocity gauge approach was successfully used for treating other laser-assisted processes [20,35–38]. Thus, our analytic expression of bound-bound atomic transition amplitudes for one-photon exchange calculated in the velocity gauge in Ref. [37] is consistent with the one reported in Ref. [39], which is calculated in the length gauge by using a method based on the Sturmian representation of the Coulomb Green's function, and in the low-frequency approximation identical analytical results for the differential cross sections were obtained within both approaches. In laser-assisted x-ray photoionization, the numerical results of the second-order amplitudes obtained in the velocity gauge as reported in Ref. [20] coincide with the ones derived in the length gauge, Ref. [19]. The choice of velocity gauge allows us to simplify the analytical calculation of the atomic transition amplitude and to report a closed-form formula of TDCS by taking advantage of exploiting the closed-form expression of radial function $\mathcal{B}_{101}$ entering in the first-order perturbed wave function of hydrogen [35,37,38].

B. The nonlinear scattering matrix

We employ a semiperturbative approach of the scattering process which is similar to that developed by Byron and Joachain [16] for free-free transitions, in which the second-order Born correction is negligible compared to the laser-dressing effects. The evaluation of the scattering amplitude is very challenging due to the complex three-body interaction: projectile electron, bound electron, and laser field. However, since we assume that both scattered and ejected electrons have large kinetic energies, the calculation simplifies, and we can derive a closed-form expression for the TDCS. Thus, the initial state of the scattering system is calculated as the product of the initial states of the fast incident electron and atomic target dressed by the laser field, $\chi_{\mathbf{k}_i}^V(\mathbf{r}_0,t)$ and $\Psi_{1s}(\mathbf{r}_1,t)$, while the final state is calculated as the product of the final states of the fast scattered and ejected electrons, which are approximated as Gordon-Volkov wave functions. Our treatment differs from that of Taïeb and coworkers [19] in the fact that we dress the fast projectile and ejected electrons to all order in the laser field and we dress the atomic target by using an atomic wave function corrected to the first order in the laser field [34]. As mentioned before, we focus our study at moderate laser intensities ($I\leqslant 1$ TW/cm^2) and fast projectile electrons (E_i, $E_f\geqslant 1$ keV) such that the interaction between the projectile electron and hydrogen atom is well treated within the first-order Born approximation in the static scattering potential $V_d(r_0,r_1)=-1/r_0+1/|\mathbf{r}_1-\mathbf{r}_0|$ for the direct channel, and $V_{\rm ex}(r_0,r_1)=-1/r_1+1/|\mathbf{r}_1-\mathbf{r}_0|$ for the exchange channel.

In order to describe the scattering process (1), we employ the direct and exchange scattering matrix elements [40], which are calculated at high kinetic energies of the projectile and ejected electrons as

$$S_{fi,d}^{B1}=-i\int_{-\infty}^{+\infty}dt\left\langle\chi_{\mathbf{k}_f}^V(\mathbf{r}_0,t)\chi_{\mathbf{k}_e}^V(\mathbf{r}_1,t)|V_d(r_0,r_1)|\times\chi_{\mathbf{k}_i}^V(\mathbf{r}_0,t)\Psi_{1s}(\mathbf{r}_1,t)\right\rangle, \quad (12)$$

$$S_{fi,\rm ex}^{B1}=-i\int_{-\infty}^{+\infty}dt\left\langle\chi_{\mathbf{k}_f}^V(\mathbf{r}_1,t)\chi_{\mathbf{k}_e}^V(\mathbf{r}_0,t)|V_{\rm ex}(r_0,r_1)|\times\chi_{\mathbf{k}_i}^V(\mathbf{r}_0,t)\Psi_{1s}(\mathbf{r}_1,t)\right\rangle, \quad (13)$$

where $\chi_{\mathbf{k}_{i(f)}}^V$ and $\chi_{\mathbf{k}_e}^V$, given by Eq. (4), represent the Gordon-Volkov wave functions of the projectile and emitted electrons embedded in the laser field, whereas Ψ_{1s}, given by Eq. (6), represents the wave function of the bound electron interacting with the laser field. By using the Jacobi-Anger identity [41],

$e^{-ix\sin\omega t} \equiv \sum_{N=-\infty}^{+\infty} J_N(x)e^{-iN\omega t}$, we expand the oscillating part of the Gordon-Volkov wave functions occurring in the scattering matrix elements, Eqs. (12) and (13), in terms of the ordinary Bessel functions of the first kind, J_N, as

$$\exp\left[-i\,\mathbf{q}\cdot\boldsymbol{\alpha}(t)\right] = \sum_{N=-\infty}^{+\infty} J_N(\mathcal{R}_q)e^{-iN\omega t+iN\phi_q}, \tag{14}$$

where the argument of the Bessel function is defined by $\mathcal{R}_q = \alpha_0|\boldsymbol{\varepsilon}\cdot\mathbf{q}|$, and ϕ_q represents the dynamical phase which is calculated as $e^{i\phi_q} = \boldsymbol{\varepsilon}\cdot\mathbf{q}/|\boldsymbol{\varepsilon}\cdot\mathbf{q}|$, where $\mathbf{q} = \mathbf{k_i} - \mathbf{k_f} - \mathbf{k_e}$ denotes the recoil momentum vector of the ionized target, H^+. Clearly, for a CP laser field a change of helicity, i.e., $\boldsymbol{\varepsilon} \to \boldsymbol{\varepsilon}^*$, leads to a change of the sign of the dynamical phase, $\phi_q \to -\phi_q$ in the TDCS, while for a LP laser field $e^{i\phi_q} = \pm 1$, and $\phi_q = n\pi$ with n an integer.

For the direct channel, by replacing Eqs. (4), (6), and (14) into Eq. (12), we obtain the scattering matrix for electron-hydrogen collisions in a laser field, after performing the integration with respect to time,

$$S^{B1}_{fi,d} = -2\pi i \sum_{N=N_{\min}}^{+\infty} \delta(E_f + E_e - E_i - E_1 - N\omega)\, T_{N,d}, \tag{15}$$

where the Dirac function, δ, assures the energy conservation, which implies that the kinetic energy of the scattered electron is determined by the relation $E_f = E_i + E_1 - E_e + N\omega$. Here the kinetic energy of the residual ion, $E_q = q^2/2m_p$, has been neglected in comparison to any of the electrons kinetic energies, E_j, ($j = i, f$, and e), since the mass of the residual ion (proton) is much larger than the electron mass. The energy spectrum of the scattered electron consists of an elastic line, $N = 0$, and a number of sidebands corresponding to the positive and negative values of N. Obviously, for a given value of the ejected electron energy, E_e, the net number of exchanged photons is limited and cannot be smaller than a minimal value that is the integer of $N_{\min} = (E_e - E_i - E_1)/\omega$.

The total nonlinear transition amplitude, $T_{N,d}$, for the laser-assisted $(e, 2e)$ ionization process in the direct channel can be split as a sum of two terms

$$T_{N,d} = T^{(0)}_{N,d} + T^{(1)}_{N,d}, \tag{16}$$

where $T^{(0)}_N$ and $T^{(1)}_N$ represent the electronic and atomic transition amplitudes. The first term on the right-hand side of the total transition amplitude Eq. (16), $T^{(0)}_N$, is the transition amplitude due to projectile electron contribution, in which the atomic dressing terms are neglected,

$$T^{(0)}_{N,d} = \frac{1}{2^{5/2}\pi^{7/2}}\frac{e^{iN\phi_q}}{\Delta^2} J_N(\mathcal{R}_q) \times \int d\mathbf{r}_1\, e^{-i\mathbf{k}_e\cdot\mathbf{r}_1}(e^{i\boldsymbol{\Delta}\cdot\mathbf{r}_1} - 1)\psi_{1s}(\mathbf{r}_1), \tag{17}$$

where the integration over the projectile coordinate, $\mathbf{r}_0$, was performed using the Bethe integral, and $\boldsymbol{\Delta} = \mathbf{k_i} - \mathbf{k_f}$ is the vector of momentum transfer from the incident to the scattered electron. After performing the radial integration with respect to $\mathbf{r}_1$ in Eq. (17), the electronic transition amplitude can be simply expressed as

$$T^{(0)}_{N,d} = -\frac{1}{(2\pi)^2} J_N(\mathcal{R}_q)\, f^{B_1}_{\rm ion}(\Delta, q, k_e)\, e^{iN\phi_q}, \tag{18}$$

where

$$f^{B_1}_{\rm ion}(\Delta, q, k_e) = -\frac{2^{5/2}}{\pi\Delta^2}\left[\frac{1}{(q^2+1)^2} - \frac{1}{\left(k_e^2+1\right)^2}\right], \tag{19}$$

is the direct scattering amplitude in the first-order plane-wave Born approximation for ionization of hydrogen atom by electron impact in the absence of the laser field [1,32]. In the electronic transition amplitude, Eq. (18), the interaction between the laser field and the projectile and ejected electrons is contained in the argument of the Bessel function $\mathcal{R}_q = (\sqrt{I}/\omega^2)|\boldsymbol{\varepsilon}\cdot\mathbf{q}|$, and phase ϕ_q, being decoupled from the kinematic term. This feature is a characteristic of employing Gordon-Volkov wave functions for fast electrons and moderate laser intensities [7,35,36]. The field-free electronic scattering amplitude $f^{B_1}_{\rm ion}$ contains a factor, $-2/\Delta^2$, which is related to the first-order Born amplitude corresponding to scattering by the Coulomb potential $-1/r_0$, while the two terms in the squared brackets of Eq. (19) are related to the momentum transfer to the residual ion, q, and the momentum of the ejected electron, k_e, respectively. For the field-free $(e, 2e)$ collisions in the plane-wave Born approximation, the first term in the right-hand side of Eq. (19) gives rise to the so-called binary encounter peak [42], which occurs at very low residual ion momentum $q \simeq 0$.

The second term on the right-hand side of Eq. (16), $T^{(1)}_N$, represents the first-order atomic transition amplitude and corresponds to processes in which the hydrogen atom absorbs or emits one photon and is subsequently ionized by the projectile electron impact. $T^{(1)}_N$ occurs due to modification of the atomic state by the laser field, the so-called *atomic dressing*, which is described by the first-order radiative correction, $\psi^{(1)}_{1s}(\mathbf{r}_1, t)$, in Eq. (7).

After some straightforward algebra, integrating over the projectile coordinate, $\mathbf{r}_0$, the direct first-order atomic transition amplitude can be written as

$$T^{(1)}_{N,d} = -\frac{\alpha_0\omega}{2}\big[J_{N-1}(\mathcal{R}_q)\,\mathcal{M}^{(1)}_{\rm at}(\omega)e^{i(N-1)\phi_q} + J_{N+1}(\mathcal{R}_q)\,\mathcal{M}^{(1)}_{\rm at}(-\omega)e^{i(N+1)\phi_q}\big], \tag{20}$$

where $\mathcal{M}^{(1)}_{\rm at}(\omega)$ denotes the specific first-order atomic transition matrix element related to one-photon absorption,

$$\mathcal{M}^{(1)}_{\rm at}(\omega) = \frac{1}{2^{5/2}\pi^{7/2}\Delta^2}\int d\mathbf{r}_1\, e^{-i\mathbf{k}_e\cdot\mathbf{r}_1}\,(e^{i\boldsymbol{\Delta}\cdot\mathbf{r}_1} - 1)\boldsymbol{\varepsilon} \cdot \mathbf{w}_{100}(E_1^+; \mathbf{r}_1), \tag{21}$$

whereas the transition matrix element $\mathcal{M}^{(1)}_{\rm at}(-\omega)$ is related to one-photon emission

$$\mathcal{M}^{(1)}_{\rm at}(-\omega) = \frac{1}{2^{5/2}\pi^{7/2}\Delta^2}\int d\mathbf{r}_1\, e^{-i\mathbf{k}_e\cdot\mathbf{r}_1}(e^{i\boldsymbol{\Delta}\cdot\mathbf{r}_1} - 1)\,\boldsymbol{\varepsilon}^* \cdot \mathbf{w}_{100}(E_1^-; \mathbf{r}_1), \tag{22}$$

where the energies $E_1^{\pm}$ are given in Eq. (10). Obviously, in Eq. (20) only one photon is exchanged (emitted or absorbed) between the laser field and the bound electron, while the

remaining $N+1$ or $N-1$ photons are exchanged between the laser field and the projectile electron. By performing the radial integral over $\mathbf{r}_1$ in Eq. (21), we derive the first-order atomic matrix element for one-photon absorption as

$$\mathcal{M}^{(1)}_{\rm at}(\omega) = -\frac{1}{2^{3/2}\pi^3\Delta^2} \times [(\boldsymbol{\varepsilon}\cdot\hat{\mathbf{q}})\,\mathcal{J}_{101}(\omega,q) - (\boldsymbol{\varepsilon}\cdot\hat{\mathbf{k}}_e)\,\mathcal{J}_{101}(\omega,-k_e)], \tag{23}$$

while the following changes are made $\omega\to-\omega$ and $\boldsymbol{\varepsilon}\to\boldsymbol{\varepsilon}^*$ in Eq. (23) to obtain the first-order atomic transition matrix element, $\mathcal{M}^{(1)}_{\rm at}(-\omega)$, for one-photon emission. The expression of the atomic radial integral $\mathcal{J}_{101}$, is given by

$$\mathcal{J}_{101}(\pm\omega,p) = \int_0^\infty dr_1\; r_1^2\; j_1(pr_1)\,\mathcal{B}_{101}(E_1^{\pm};r_1), \tag{24}$$

with $\mathcal{J}_{101}(\omega,-p) = -\mathcal{J}_{101}(\omega,p)$, where $p=q$ or k_e. After performing some algebra in Eq. (24), by using the expansion of the spherical Bessel function, j_1, an analytical form of the radial integral is obtained in terms of two Appell's hypergeometric function, F_1, as

$$\mathcal{J}_{101}(\omega,p) = \frac{2^6\tau}{p\,(2-\tau)(1+\tau)^4}\mathrm{Re}\Big[a^3F_1(b,1,3,b+1,x,y) - \frac{ia^2}{2p}F_1(b,2,2,b+1,x,y)\Big], \tag{25}$$

in which $a=\tau/(1+ip\tau)$, $b=2-\tau$, and the variables of the Appell's hypergeometric function are

$$x=\frac{\tau-1}{\tau+1},\quad y=\frac{(1-\tau)(1-ip\tau)}{(1+\tau)(1+ip\tau)}, \tag{26}$$

where the parameter τ depends on the photon energy, ω, and it takes two values, $\tau^- = 1/\sqrt{-2E_1^+}$ and $\tau^+ = 1/\sqrt{-2E_1^-}$, corresponding to the two energies E_1^+ and E_1^- defined in Eq. (10).

The first-order atomic matrix element, Eq. (23), has a structure that explicitly contains the scalar products $\boldsymbol{\varepsilon}\cdot\hat{\mathbf{q}}$ and $\boldsymbol{\varepsilon}\cdot\hat{\mathbf{k}}_e$, depends on the scattering geometry, being written in a closed form that allows us to analyze the dependence on the laser field polarization. The last term in the right-hand side of the electronic scattering amplitude and atomic matrix element, Eqs. (19) and (23), occurs due to the nonorthogonality of the Gordon-Volkov wave function of the ejected electron and the initial ground-state wave function of the hydrogen atom. The structure of Eq. (23) is also similar to other processes, with the vectors $\mathbf{q}$ and $\mathbf{k}_e$ replaced by vectors which are specific to each particular process, such as elastic laser-assisted scattering of electrons by hydrogen atoms [37,43], bremsstrahlung cross sections in the electron-hydrogen atom collisions [39], or laser-assisted electron-impact excitation of hydrogen atoms [36].

C. The nonlinear scattering matrix for exchange scattering

Our formalism does not neglect the exchange effects between the scattered and ejected electrons in both the electronic and atomic terms, since fast incident and outgoing electrons are involved in the calculation, and, as in the EMS experiments, their kinetic energies could have comparable orders of magnitude. We notice from Eq. (13) that the exchange scattering matrix is obtained from the direct one, Eq. (12), by interchanging the position coordinates of the two outgoing electrons, $\mathbf{r}_1$ and $\mathbf{r}_0$, in the Gordon-Volkov wave functions $\chi^V_{\mathbf{k}_f}$ and $\chi^V_{\mathbf{k}_e}$, as well in the direct potential V_d. In the first-order Born approximation in the exchange potential, $V_{\rm ex}$, we obtain the exchange scattering matrix for the laser-assisted $(e,2e)$ reactions, after performing the integration with respect to time in Eq. (13),

$$S^{B1}_{fi,\rm ex} = -2\pi i\sum_{N=N_{\rm min}}^{+\infty}\delta(E_f+E_e-E_i-E_1-N\omega)\,T_{N,\rm ex}, \tag{27}$$

where the total nonlinear transition amplitude for the exchange channel can be split as a sum of two terms $T_{N,\rm ex} = T^{(0)}_{N,\rm ex} + T^{(1)}_{N,\rm ex}$. The electronic transition amplitude for the exchange scattering, $T^{(0)}_{N,\rm ex}$, in which the atomic dressing contribution is neglected, can be expressed as

$$T^{(0)}_{N,\rm ex} = \frac{1}{2^{5/2}\pi^{7/2}}\frac{e^{iN\phi_q}}{\Delta_e^2}J_N(\mathcal{R}_q)\int d\mathbf{r}_1\; e^{i\mathbf{q}\cdot\mathbf{r}_1}\psi_{1s}(\mathbf{r}_1), \tag{28}$$

where the integration over the position coordinate, $\mathbf{r}_0$, was performed. After performing the radial integration with respect to $\mathbf{r}_1$, the exchange electronic transition amplitude can be simply expressed as

$$T^{(0)}_{N,\rm ex} = -\frac{1}{(2\pi)^2}J_N(\mathcal{R}_q)\,g^{B_1}_{\rm ion,ex}(\Delta_e,q)\;e^{iN\phi_q}, \tag{29}$$

where

$$g^{B_1}_{\rm ion,ex}(\Delta_e,q) = -\frac{2^{5/2}}{\pi\,\Delta_e^2(q^2+1)^2} \tag{30}$$

denotes the electronic exchange amplitude in the absence of the laser field, that is in agreement with the Born-Ochkur approximation [40,44], and Δ_e represents the amplitude of the momentum transfer vector from the incident to the ejected electron, $\boldsymbol{\Delta}_e = \mathbf{k}_i - \mathbf{k}_e$. We mention that only the interelectronic interaction, $1/|\mathbf{r}_1-\mathbf{r}_0|$, contributes to the exchange transition amplitude $T_{N,\rm ex}$, and the exchange scattering amplitude $g^{B_1}_{\rm ion,ex}(\Delta_e,q)$ can be obtained from the direct one $f^{B_1}_{\rm ion}(\Delta,q,k_e)$ by interchanging k_f and k_e, and dropping the $-1/r_0$ interaction in the direct potential, because the electron-nucleus interaction term $-1/r_1$ of the exchange scattering potential gives zero contribution to Eq. (13).

Similarly to the direct scattering, the first-order atomic transition amplitude for the exchange scattering can be expressed as

$$T^{(1)}_{N,ex} = -\frac{\alpha_0\omega}{2}\big[J_{N-1}(\mathcal{R}_q)\,\mathcal{M}^{(1)}_{\rm at,ex}(\omega)e^{i(N-1)\phi_q} + J_{N+1}(\mathcal{R}_q)\,\mathcal{M}^{(1)}_{\rm at,ex}(-\omega)e^{i(N+1)\phi_q}\big], \tag{31}$$

where $\mathcal{M}^{(1)}_{\rm at,ex}(\omega)$ denotes the specific first-order atomic transition matrix element for the exchange scattering, related to one-photon absorption

$$\mathcal{M}^{(1)}_{\rm at,ex}(\omega) = \frac{1}{2^{5/2}\pi^{7/2}\Delta_e^2}\int d\mathbf{r}_1\; e^{i\mathbf{q}\cdot\mathbf{r}_1}\boldsymbol{\varepsilon}\cdot\mathbf{w}_{100}(E_1^+;\mathbf{r}_1), \tag{32}$$

whereas $\mathcal{M}^{(1)}_{\rm at,ex}(-\omega)$ is related to one-photon emission and can be obtained from $\mathcal{M}^{(1)}_{\rm at,ex}(\omega)$ by changing $\omega \to -\omega$ and $\boldsymbol{\varepsilon} \to \boldsymbol{\varepsilon}^*$. By performing the radial integral over $\mathbf{r}_1$ in Eq. (32), we obtain

$$\mathcal{M}^{(1)}_{\rm at,ex}(\pm\omega) = -\frac{\boldsymbol{\varepsilon}\cdot\hat{\mathbf{q}}}{2^{3/2}\pi^3\Delta_e^2}\,\mathcal{J}_{101}(\pm\omega, q), \tag{33}$$

where $\mathcal{J}_{101}(\pm\omega, q)$ is calculated from Eq. (25). It turns out that the exchange effects for both electronic and atomic contributions to the transition amplitude vary like Δ_e^{-2}, and cannot be neglected in comparison to the contribution of the direct scattering channel if the momentum transfers Δ_e and Δ are comparable in magnitude (indistinguishable electrons) or $\Delta_e \leqslant \Delta$. In contrast, for very fast incident and scattered electrons, $E_{i(f)} \gg 1$ a.u., and slow ejected electrons, $E_e \ll E_f$, the electronic and atomic contributions due to exchange channel can be safely neglected compared to the ones for the corresponding direct process.

D. The low-photon energy approximation

In the low-photon energy limit where the photon energy is small compared to the ionization energy of the hydrogen atom (typically in the infrared region), it is worth presenting some useful simple approximation formulas for the atomic transition amplitude. In most theoretical works, the analytical calculations cannot be done exactly and, as the photon energy remains small, it is expected that only few intermediate bound states to contribute to the atomic transition amplitude and thus to approximate the complicated analytical formulas. This is the key of the closure approximation method [16], which consists in replacing the difference energy $E_n - E_1$ by an average excitation energy $\bar{\omega} \simeq 4/9$ a.u. for the hydrogen atom in approximating the sum over the intermediate states in the atomic transition amplitudes. Here we present a different approach based on the low-frequency approximation (LFA), given by the lowest order term of the expansion of the atomic matrix element $\mathcal{M}^{(1)}_{\rm at}(\omega)$ in powers of the laser photon energy. After some algebra, we derive an approximate formula for the atomic radial integral, $\mathcal{J}_{101}$, in the low-photon energy limit $\omega \ll |E_1|$ in Eq. (25), in the first order in ω,

$$\mathcal{J}_{101}(\omega, p) \simeq -\frac{16\,p}{(p^2+1)^3}\left(1 - \frac{\omega}{2}\,\frac{p^2-9}{p^2+1}\right), \tag{34}$$

where $p = q$ or k_e, and, therefore the atomic transition amplitude for the direct process, Eq. (20), in the low-photon energy limit reads as

$$T^{(1)}_{N,d} \simeq \alpha_0\omega\frac{2^{3/2}e^{iN\phi_q}}{\pi^3\Delta^2}\left\{J_{N-1}(\mathcal{R}_q)e^{-i\phi_q}\left[\frac{\boldsymbol{\varepsilon}\cdot\mathbf{q}}{(q^2+1)^3} + \frac{\boldsymbol{\varepsilon}\cdot\mathbf{k}_e}{\left(k_e^2+1\right)^3}\right] + J_{N+1}(\mathcal{R}_q)e^{i\phi_q}\left[\frac{\boldsymbol{\varepsilon}^*\cdot\mathbf{q}}{(q^2+1)^3} + \frac{\boldsymbol{\varepsilon}^*\cdot\mathbf{k}_e}{\left(k_e^2+1\right)^3}\right]\right.$$
$$\left. + \frac{\omega}{2}J_{N-1}(\mathcal{R}_q)e^{-i\phi_q}\left[\frac{\boldsymbol{\varepsilon}\cdot\mathbf{q}\,(q^2-9)}{(q^2+1)^4} + \frac{\boldsymbol{\varepsilon}\cdot\mathbf{k}_e\left(k_e^2-9\right)}{\left(k_e^2+1\right)^4}\right] - \frac{\omega}{2}J_{N+1}(\mathcal{R}_q)e^{i\phi_q}\left[\frac{\boldsymbol{\varepsilon}^*\cdot\mathbf{q}\,(q^2-9)}{(q^2+1)^4} + \frac{\boldsymbol{\varepsilon}^*\cdot\mathbf{k}_e\left(k_e^2-9\right)}{\left(k_e^2+1\right)^4}\right]\right\}. \tag{35}$$

For a LP laser field, the following formula holds, $J_N(\mathcal{R}_q) = J_N(\alpha_0\,\boldsymbol{\varepsilon}\cdot\mathbf{q})e^{-iN\phi_q}$, and we obtain from Eqs. (18) and (19) the direct electronic transition amplitude,

$$T^{(0),\rm LP}_{N,d} = \frac{2^{1/2}}{\pi^3\Delta^2}J_N(\alpha_0\,\boldsymbol{\varepsilon}\cdot\mathbf{q})\left[\frac{1}{(q^2+1)^2} - \frac{1}{\left(k_e^2+1\right)^2}\right], \tag{36}$$

and the direct atomic transition amplitude, Eq. (35), simplifies to

$$T^{(1),\rm LP}_{N,d} \simeq \frac{2^{5/2}}{\pi^3}\,\frac{\omega}{\Delta^2}\left\{NJ_N(\alpha_0\,\boldsymbol{\varepsilon}\cdot\mathbf{q})\left[\frac{1}{(q^2+1)^3} + \frac{\boldsymbol{\varepsilon}\cdot\mathbf{k}_e}{\boldsymbol{\varepsilon}\cdot\mathbf{q}}\,\frac{1}{\left(k_e^2+1\right)^3}\right] + \frac{\alpha_0\omega}{2}J'_N(\alpha_0\,\boldsymbol{\varepsilon}\cdot\mathbf{q})\left[\frac{\boldsymbol{\varepsilon}\cdot\mathbf{q}\,(q^2-9)}{(q^2+1)^4} + \frac{\boldsymbol{\varepsilon}\cdot\mathbf{k}_e\left(k_e^2-9\right)}{\left(k_e^2+1\right)^4}\right]\right\}, \tag{37}$$

where we have used the recurrence relation $J_{N-1}(x) + J_{N+1}(x) = J_N(x)(2N/x)$, and J'_N is the first derivative of the Bessel function which satisfies the relation $J'_N(x) = [J_{N-1}(x) - J_{N+1}(x)]/2$, with $x = \alpha_0(\boldsymbol{\varepsilon}\cdot\mathbf{q})$, [41]. If we consider the lowest order in the photon energy ω in Eq. (37)

$$T^{(1),\rm LP}_{N,d} \simeq \frac{2^{5/2}}{\pi^3}\,\frac{N\omega}{\Delta^2}J_N(\alpha_0\,\boldsymbol{\varepsilon}\cdot\mathbf{q}) \times\left[\frac{1}{(q^2+1)^3} + \frac{\boldsymbol{\varepsilon}\cdot\mathbf{k}_e}{\boldsymbol{\varepsilon}\cdot\mathbf{q}}\,\frac{1}{\left(k_e^2+1\right)^3}\right], \tag{38}$$

we obtain the LFA formula for N-photon absorption atomic transition element in the case of a LP field. However, in the limit $\omega \to 0$ for scattering parameters such that $\mathcal{R}_q \gg 1$, i.e., where there is a strong coupling between the projectile and ejected electrons and the laser field, the transition amplitudes derived in the semiperturbative approach do not diverge, but approach the zero value, due to asymptotic behavior of the Bessel function of the first kind [41] at large arguments, $J_N(x) \simeq \sqrt{2/\pi x}\cos(x - N\pi/2 - \pi/4)$, for $x \to \infty$.

Furthermore, whenever the condition $\mathcal{R}_q \ll 1$ is satisfied, i.e., the perturbative regime of low laser intensities where $\alpha_0 \ll 1$ a.u. and/or scattering kinematics with $|\boldsymbol{\varepsilon}\cdot\mathbf{q}| \ll 1$ a.u., we can use the approximate formula for the Bessel function at small arguments,

$$J_N(\mathcal{R}_q) \simeq \frac{1}{N!}\left(\frac{\mathcal{R}_q}{2}\right)^N, \quad \text{for} \quad N > 0, \tag{39}$$

and $J_N(\mathcal{R}_q) = (-1)^{-N} J_{-N}(\mathcal{R}_q)$, for $N \leqslant 0$ [41]. Thus, in the perturbative region with $\mathcal{R}_q \ll 1$, we obtain from Eq. (36) a simple formula for the direct electronic transition amplitude for N-photon absorption ($N > 0$), as

$$T_{N,d}^{(0),\mathrm{LP}} \simeq \alpha_0^N \frac{2^{1/2}}{\pi^3 \Delta^2 N!} \left(\frac{\boldsymbol{\varepsilon}\cdot\mathbf{q}}{2}\right)^N \left[\frac{1}{(q^2+1)^2} - \frac{1}{\left(k_e^2+1\right)^2}\right], \tag{40}$$

while for the direct atomic transition amplitude for N-photon absorption in the LFA we obtain from Eq. (38)

$$T_{N,d}^{(1),\mathrm{LP}} \simeq \alpha_0^N \frac{2^{5/2} N\omega}{\pi^3 \Delta^2 N!} \left(\frac{\boldsymbol{\varepsilon}\cdot\mathbf{q}}{2}\right)^N \times \left[\frac{1}{(q^2+1)^3} + \frac{\boldsymbol{\varepsilon}\cdot\mathbf{k}_e}{\boldsymbol{\varepsilon}\cdot\mathbf{q}} \frac{1}{\left(k_e^2+1\right)^3}\right]. \tag{41}$$

Expressions similar to Eqs. (36) and (37) and Eqs. (40) and (41) can be easily derived for the exchange scattering channel. As expected, the electronic and atomic transition amplitudes are important at scattering and ejected angles where the momenta q, Δ, and Δ_e are small. The ratio of the direct atomic and electronic transition amplitudes derived in the low-photon energy limit, Eqs. (41) and (40),

$$\frac{T_{N,d}^{(1),\mathrm{LP}}}{T_{N,d}^{(0),\mathrm{LP}}} \simeq \frac{4N\omega}{q^2+1}\left[1 + \frac{(q^2+1)^3}{\left(k_e^2+1\right)^3}\frac{\boldsymbol{\varepsilon}\cdot\mathbf{k}_e}{\boldsymbol{\varepsilon}\cdot\mathbf{q}}\right] \times \left[1 - \frac{(q^2+1)^2}{\left(k_e^2+1\right)^2}\right]^{-1}, \tag{42}$$

shows that, compared to the projectile electron contribution, the first-order atomic dressing effects for $\omega \ll 1$ a.u. and laser parameters such that $\mathcal{R}_q \ll 1$, are increasing with the net number of exchanged photons, N, and photon energy, ω, and are decreasing with the momenta of the ejected electron, k_e, and residual ion, q. Obviously, Eq. (42) shows that differences occur in the TDCSs for absorption or emission of N photons, which correspond to positive or negatives values of N, due to constructive or destructive interferences of the electronic and atomic terms in TDCS.

In the case of one-photon absorption ($N = 1$) in the perturbative regime with $\mathcal{R}_q \ll 1$ and low photon energies, we can use the approximate formula for the Bessel function, Eq. (39), and by keeping only the first order in laser field intensity, I, we obtain simple formulas for the direct electronic transition amplitude, Eq. (18),

$$T_{N=1,d}^{(0)} \simeq \frac{\sqrt{I}}{2^{1/2}\pi^3} \frac{\boldsymbol{\varepsilon}\cdot\mathbf{q}}{\omega^2\Delta^2}\left[\frac{1}{(q^2+1)^2} - \frac{1}{\left(k_e^2+1\right)^2}\right], \tag{43}$$

as well for the direct atomic transition amplitude derived in the low-photon energy limit, Eq. (35),

$$T_{N=1,d}^{(1)} \simeq \frac{2^{3/2}}{\pi^3}\frac{\sqrt{I}}{\omega\Delta^2}\left[\frac{\boldsymbol{\varepsilon}\cdot\mathbf{q}}{(q^2+1)^3}\left(1 + \frac{\omega}{2}\frac{q^2-9}{q^2+1}\right) + \frac{\boldsymbol{\varepsilon}\cdot\mathbf{k}_e}{\left(k_e^2+1\right)^3}\left(1 + \frac{\omega}{2}\frac{k_e^2-9}{k_e^2+1}\right)\right]. \tag{44}$$

Moreover, if we keep the lowest order in the photon energy in Eq. (44), we obtain a quite simple formula for the direct atomic transition amplitude

$$T_{N=1,d}^{(1)} \simeq \frac{2^{3/2}}{\pi^3}\frac{\sqrt{I}}{\omega\Delta^2}\left[\frac{\boldsymbol{\varepsilon}\cdot\mathbf{q}}{(q^2+1)^3} + \frac{\boldsymbol{\varepsilon}\cdot\mathbf{k}_e}{\left(k_e^2+1\right)^3}\right], \tag{45}$$

in the LFA for one-photon absorption in the perturbative regime.

Similarly, for the exchange scattering, we derive simple approximate formulas for the electronic and atomic transition amplitudes at $\mathcal{R}_q \ll 1$, Eqs. (29) and (31) in the low-photon energy limit, as

$$T_{N=1,\mathrm{ex}}^{(0)} \simeq \frac{1}{2^{1/2}\pi^3}\frac{\sqrt{I}}{\omega^2\Delta_e^2}\frac{\boldsymbol{\varepsilon}\cdot\mathbf{q}}{(q^2+1)^2}, \tag{46}$$

$$T_{N=1,\mathrm{ex}}^{(1)} \simeq \frac{2^{3/2}}{\pi^3}\frac{\sqrt{I}}{\omega\Delta_e^2}\frac{\boldsymbol{\varepsilon}\cdot\mathbf{q}}{(q^2+1)^3}\left(1 + \frac{\omega}{2}\frac{q^2-9}{q^2+1}\right). \tag{47}$$

The infrared divergence in the limit $\omega \to 0$ is evident in all the above electronic and atomic transition amplitude expressions derived at $\mathcal{R}_q \ll 1$. Thus, in the perturbative regime and low-photon energy approximation the electronic transition amplitude varies like ω^{-2}, while the atomic transition amplitude varies like ω^{-1}, which is reminiscent of the infrared divergence of quantum electrodynamics [45] and Low theorem [46] in the limit $\omega \to 0$. Clearly, these simple analytical formulas we have derived for one-photon absorption, as well for nonlinear atomic transition amplitudes, might provide more physical insight into the laser-assisted $(e, 2e)$ reactions.

E. The triple differential cross section

It is well known that the TDCS can provide useful information about collision dynamics in the electron-impact ionization process [7]. For laser-assisted $(e, 2e)$ collisions accompanied by the transfer of N photons, we calculate the nonlinear TDCS in the first-order Born approximation in the scattering potential, for unpolarized incident projectile and hydrogen beams, and without distinguishing between the final spin states of the electrons,

$$\frac{d^3\sigma_N^{B1}}{d\Omega_f\, d\Omega_e\, dE_f} = (2\pi)^4 \frac{k_f k_e}{k_i} \times \left(\tfrac{1}{4}|T_{N,d} + T_{N,\mathrm{ex}}|^2 + \tfrac{3}{4}|T_{N,d} - T_{N,\mathrm{ex}}|^2\right), \tag{48}$$

averaged over the initial spin states and summed over the final spin states. The projectile electrons are scattered into the solid angle Ω_f and $\Omega_f + d\Omega_f$ with the kinetic energy between E_f and $E_f + dE_f$, and the ejected electrons are emitted within the solid angle Ω_e and $\Omega_e + d\Omega_e$. The TDCS is a function of the electrons momentum vectors $\mathbf{k}_i$, $\mathbf{k}_f$, and $\mathbf{k}_e$, and depends on the laser parameters: intensity I, photon energy ω, and polarization $\boldsymbol{\varepsilon}$. The dominant contribution to TDCS is due to collisions involving small momentum transfers Δ and Δ_e, small momentum of the residual ion q, or near resonance photon energies. The TDCS for the laser-assisted $(e, 2e)$ process

is given by

$$\frac{d^3\sigma^{B1}}{d\Omega_f\, d\Omega_e\, dE_f} = \sum_{N=N_{\min}}^{+\infty} \frac{d^3\sigma_N^{B1}}{d\Omega_f\, d\Omega_e\, dE_f}. \tag{49}$$

By integrating TDCS over the direction of the scattered electrons, Ω_f, we obtain the double differential cross section of the ejected electrons, while by integrating TDCS over the direction of the ejected electrons, Ω_e, we derive the double differential cross section of the scattered electrons. Finally, the total ionization cross section is deduced by integrating over the angles and energies of the scattered and ejected electrons.

In the limit of very weak laser fields with $\alpha_0 \ll 1$ a.u. and low-photon energies with $\omega \ll E_i$, by neglecting the atomic dressing in Eq. (48), namely $T_{N,d}^{(1)} \simeq 0$ and $T_{N,ex}^{(1)} \simeq 0$, we obtain the Kroll-Watson approximation of laser-assisted $(e, 2e)$ process, in which TDCS is written as

$$\frac{d^3\sigma_N^{B1}}{d\Omega_f\, d\Omega_e\, dE_f} = \frac{k_f}{k_{f,0}} \frac{k_e}{k_{e,0}} |J_N(\mathcal{R}_q)|^2 \frac{d^3\sigma_{FF}^{B1}}{d\Omega_f\, d\Omega_e\, dE_f}, \tag{50}$$

where $k_{f(e),0}$ are the scattered and ejected electron momentum in the absence of the laser field and $d^3\sigma_{FF}^{B1}/d\Omega_f\, d\Omega_e\, dE_f$ is the field-free TDCS in the first-order Born approximation. Moreover, at small momentum of the residual ion, $q \ll k_e$, we obtain a simple formula for the laser-assisted TDCS,

$$\frac{d^3\sigma_N^{B1}}{d\Omega_f\, d\Omega_e\, dE_f} \simeq \frac{k_f k_e}{k_i} |J_N(\mathcal{R}_q)|^2 \frac{4}{\Delta^4} \times \left(1 - \frac{\Delta^2}{\Delta_e^2} + \frac{\Delta^4}{\Delta_e^4}\right) \left|\psi_{1s}^{(0)}(q)\right|^2, \tag{51}$$

that "decouples" into a product of three factors: (i) the squared Bessel function which includes the laser-projectile and ejected electrons interaction, (ii) the electron-electron collision factor in the first-order Born approximation

$$f_{ee}^{B1} = \frac{1}{4\pi^4\Delta^4}\left(1 - \frac{\Delta^2}{\Delta_e^2} + \frac{\Delta^4}{\Delta_e^4}\right),$$

that is the absolute square of the half-off-shell Coulomb-matrix element summed and averaged over final and initial spin states for fast projectile and outgoing electrons [47], and (iii) $|\psi_{1s}^{(0)}(q)|^2 = 8\pi^{-2}(q^2+1)^{-4}$ that represents the squared momentum-space wave function for the ground state of atomic hydrogen [1]. Equation (51) is in agreement to the TDCS derived for EMS by Kouzakov and coworkers, namely Eq. (26) in Ref. [22]. The half-off-shell Mott scattering TDCS, for fast projectile and outgoing electrons that includes the exchange terms [4,40], is simply calculated as $(2\pi)^4 f_{ee}^{B1}$,

$$\left(\frac{d\sigma}{d\Omega_e}\right)_{ee} = \frac{4}{\Delta^4}\left(1 - \frac{\Delta^2}{\Delta_e^2} + \frac{\Delta^4}{\Delta_e^4}\right). \tag{52}$$

If we take into account the atomic dressing in Eq. (48) in the low-photon energy limit $\omega \ll |E_1|$, and consider the lowest order in the photon energy in Eq. (35), at small momentum of the residual ion, $q \ll k_e$, we obtain

$$\frac{d^3\sigma_N^{B1}}{d\Omega_f\, d\Omega_e\, dE_f} \simeq \frac{k_f k_e}{k_i} |J_N(\mathcal{R}_q)|^2 \left(\frac{d\sigma}{d\Omega_e}\right)_{ee} \times \left(1 + \frac{4N\omega}{q^2+1}\right)^2 \left|\psi_{1s}^{(0)}(q)\right|^2, \tag{53}$$

that is in agreement to the laser-assisted TDCS derived in the low-photon energy approximation for EMS by Bulychev and coworkers, namely Eqs. (9)–(11) in Ref. [23]. In contrast to Eq. (51) in which the atomic dressing effects are neglected, the TDCS Eq. (53) does not obey the well-known Kroll-Watson sum rule [48]. Obviously, the TDCS in the laser-assisted $(e, 2e)$ collisions provides valuable information about the collision dynamics [4], electronic structure of the target, and can be used to derive the momentum density distribution of the target electron, which was first demonstrated for hydrogen and helium atoms [1,30].

III. NUMERICAL EXAMPLES AND DISCUSSION

In this section, we present our numerical results for the laser-assisted electron-impact ionizing collisions in hydrogen, described by Eq. (1), for fast incident and outgoing electrons, and we apply the semiperturbative formulas derived in Sec. II to calculate the nonlinear TDCSs in the presence of a LP laser field. Obviously, due to the complicated analytical form of the laser-dressed atomic wave function, the total scattering amplitude has to be numerically evaluated. It is worth pointing out that the electronic and atomic transition amplitudes, Eqs. (18), (20), (29), and (31), as well their approximations derived in Subsec. II D are applicable for arbitrary scattering configurations and laser field polarizations.

We study the laser-assisted $(e, 2e)$ process in the coplanar geometry depicted in Fig. 1, in which the momenta of the electrons, $\mathbf{k}_i$, $\mathbf{k}_f$, and $\mathbf{k}_e$, lie in the same plane where the two outgoing electrons are detected in coincidence at the scattering angles θ_f and θ_e, with equal corresponding azimuthal angles $\varphi_f = \varphi_e = \varphi_i$. The momentum vector of the incident electron, $\mathbf{k}_i$, is taken parallel to the z axis, with $\theta_i = 0^\circ$ and $\varphi_i = 0^\circ$, and the scattering angle θ_f of the scattered electron is fixed, while the angle θ_e of the ejected electron is varied. The asymmetric scattering geometry is considered in which $\theta_f \neq \theta_e$ and $k_f \neq k_e$. At this point, it is useful to recall the differences between the symmetric and asymmetric scattering geometries, namely the symmetric geometry is defined by the requirement that the scattering angles and energies of the scattered and ejected electrons are equal. In a kinematically complete experiment by measuring the momentum vectors of both ejected electron and ionized target, $\mathbf{k}_e$ and $\mathbf{q}$, we can deduce the momentum of the scattered electron, $\mathbf{k}_f = \mathbf{k}_i - \mathbf{k}_e - \mathbf{q}$, as well as the momentum transfer of the scattered electron, $\mathbf{\Delta} = \mathbf{k}_i - \mathbf{k}_f$, occurring during the collision [8].

Thus, from the energy conservation law, the final momentum of the projectile is given by $k_f = (k_i^2 - k_e^2 + 2E_1 + 2N\omega)^{1/2}$, while the momentum transfer of the projectile is simple calculated as $\Delta = (k_i^2 + k_f^2 - 2k_i k_f \cos\theta_f)^{1/2}$. The Cartesian components of the momentum transfer vector, $\mathbf{\Delta}$, are given by $(-k_f \sin\theta_f, 0, k_i - k_f\cos\theta_f)$ and the amplitude Δ varies in the range $|k_i - k_f| \leqslant \Delta \leqslant k_i + k_f$, for forward $\theta_f = 0^\circ$ and backward $\theta_f = 180^\circ$ scattering, respectively. Similarly, the amplitude of the momentum transfer vector $\mathbf{\Delta}_e$ is calculated as $\Delta_e = (k_i^2 + k_e^2 - 2k_i k_e \cos\theta_e)^{1/2}$. The amplitude of the

recoil momentum vector of the residual ion, q, is given by

$$q = \left[\Delta^2 + k_e^2 - 2k_i k_e \cos\theta_e + 2k_f k_e \cos(\theta_f - \theta_e)\right]^{1/2}. \quad (54)$$

The argument $\mathcal{R}_q$ of the Bessel functions is calculated as

$$\mathcal{R}_q^2 = \mathcal{R}_i^2 + \mathcal{R}_f^2 + \mathcal{R}_e^2 - 2\mathcal{R}_i\mathcal{R}_f \cos(\phi_i - \phi_f) - 2\mathcal{R}_i\mathcal{R}_e \cos(\phi_i - \phi_e) + 2\mathcal{R}_f\mathcal{R}_e \cos(\phi_f - \phi_e),$$

where $\mathcal{R}_s = \alpha_0|\boldsymbol{\varepsilon}\cdot\mathbf{k}_s|$ and $e^{i\phi_s} = \boldsymbol{\varepsilon}\cdot\mathbf{k}_s/|\boldsymbol{\varepsilon}\cdot\mathbf{k}_s|$, with $s = i, f$, and e. For a LP laser field, the dependence of $\mathcal{R}_s$ on the laser polarization is given by $\mathcal{R}_s = \alpha_0|\mathbf{e}_j\cdot\mathbf{k}_s|$ and $\phi_s = n\pi$, while for a CP field with the polarization unit vector $\boldsymbol{\varepsilon} = (\mathbf{e}_j + i\mathbf{e}_l)/\sqrt{2}$, we obtain $\mathcal{R}_s = (\alpha_0/\sqrt{2})\sqrt{(\mathbf{e}_j\cdot\mathbf{k}_s)^2 + (\mathbf{e}_l\cdot\mathbf{k}_s)^2}$ and $\phi_s = \arctan(\mathbf{e}_l\cdot\mathbf{k}_s)/(\mathbf{e}_j\cdot\mathbf{k}_s) + n\pi$, where n is an integer. In our numerical calculation, we consider that the laser field is linearly polarized in the same direction along the momentum vector of the incident electron, $\boldsymbol{\varepsilon}||\mathbf{k}_i$. Specifically, for a LP laser field and a coplanar scattering geometry with $\phi_i = \phi_f = \phi_e = 0^\circ$ the argument of the Bessel function simplifies to $\mathcal{R}_q = \alpha_0(k_i - k_f\cos\theta_f - k_e\cos\theta_e)^{1/2}$.

To start with, we have checked that the numerical results of TDCSs for the $(e, 2e)$ scattering of fast electrons by hydrogen atoms in their ground state are in agreement with earlier numerical data published in the literature. A very good agreement is obtained with the numerical results of TDCS for one- and two-photon exchange presented in Fig. 1 of Ref. [22] and Figs. 1 and 2 of Ref. [23], under the kinematical conditions of EMS (small momentum of the residual ion q and large momentum transfers Δ and Δ_e), for incident electrons of kinetic energy $E_i = 2013.6$ eV, in a noncoplanar symmetric scattering geometry, and a LP laser of intensity 4×10^{12} W/cm^2, calculated in the low-frequency approximation at $\omega = 1.17$ eV. At an incident electron kinetic energy $E_i = 500$ eV, in a coplanar symmetric geometry, $\boldsymbol{\varepsilon}\|\boldsymbol{\Delta}$, and a LP laser of intensities $I = 1.3\times10^7$ W/cm^2, $10^2\times I$, $10^4\times I$, and $10^6\times I$, the behavior of the TDCS calculated from Eq. (48) is in fair agreement, up to a scaling factor, to the first-order Born calculation of TDCS for the ionization of hydrogen shown in Figs. 2 and 3 of Ref. [24]. Since the atomic wave function was calculated within the closure approximation [24], our numerical results disagree at larger photon energies $\omega > 3$ eV where the atomic dressing effect is more important and cannot be accurately described by this approximation. At the resonance photon energy of 10.2 eV, laser intensity of 1.3×10^7 W/cm^2, and polarization $\boldsymbol{\varepsilon}||\boldsymbol{k}_i$, in the Ehrhardt asymmetric coplanar geometry, with the incident and ejected electrons kinetic energies $E_i = 250$ eV and $E_e = 5$ eV, and scattering angle $\theta_f = 3^\circ$, the TDCS given by Eq. (48) is in an satisfactory agreement with the first-Born TDCS for the ionization of hydrogen plotted in Fig. 3(a) of Ref. [19], where the atomic wave function is calculated using a Coulomb-Sturmian basis. Obviously, despite the low value of the ejected electron kinetic energy, the agreement is due to the fact that for one-photon resonance the TDCS is dominated by the atomic contribution due to $1s$-$2p$ excitation.

Now, we return our discussion to the scattering geometry depicted in Fig. 1, where the laser polarization, $\boldsymbol{\varepsilon}$, is parallel to the incident electron momentum direction, $\mathbf{k}_i$, and the outgoing electrons move asymmetrically with respect to the direction of the incident electron, with different scattering and ejected angles, and different kinetic energies. We have chosen high kinetic energies of the projectile and ejected electrons (compared to the atomic scale), moderate laser intensities below 1 T W/cm^2 which correspond to electric field strengths lower than 2.7×10^7 V/cm, and have considered photon energies below the ionization threshold of the hydrogen atom. Specifically, a laser intensity of 1 T W/cm^2 and a photon energy of 1.55 eV (Ti:sapphire laser) result in a quiver motion amplitude $\alpha_0 \simeq 1.64$ a.u. and an argument of the ordinary Bessel function $\mathcal{R}_q \simeq 1.64|\boldsymbol{\varepsilon}\cdot\mathbf{q}|$, while for a larger photon energy of 3.1 eV (Ti:sapphire second harmonic) the corresponding amplitude α_0 and the argument $\mathcal{R}_q$ are about four times smaller. The numerical results obtained for TDSCs in the first-order Born approximation in the scattering potential, Eq. (48), are compared with those obtained by considering the atomic contribution in the LFA, Eq. (38), and those obtained by neglecting the dressing of the target by setting $T_{N,d}^{(1)} \simeq 0$ and $T_{N,ex}^{(1)} \simeq 0$ in Eq. (48).

In Fig. 2, we present the TDCSs as a function of the angle of the ejected electron, θ_e, with exchange of one photon, $N = 1$, at high kinetic energies of the projectile electron $E_i = 2$ keV and ejected electron $E_e = 200$ eV, and a small scattering angle, $\theta_f = 5^\circ$. The laser intensity is $I = 1$ T W/cm^2, while the photon energies we consider are 1.55 eV in Fig. 2(a), 3.1 eV in Fig. 2(b), 4.65 eV in Fig. 2(c), and 9.3 eV in Fig. 2(d). Figures 2(e)–2(h) illustrate, in a logarithmic scale, the same results of the laser-assisted TDCSs as in Figs. 2(a)–2(d) together with the field-free TDCSs, which are represented by the dotted lines. Figure 3 show similar results to Fig. 2, but for a larger scattering angle $\theta_f = 15^\circ$. In all figures, the solid lines correspond to the laser-assisted TDCSs calculated from Eq. (48), which include the laser dressing effects of the projectile and of the hydrogen atom, the dot-dashed lines correspond to the TDCSs in which the atomic dressing is considered in the LFA for the direct and as well as exchange scattering, while the dashed lines correspond to the results in which the atomic dressing is neglected.

As resulted from our theoretical calculations, the TDCS is quite important at scattering and ejected angles where the recoil momentum q is small. Thus, at the scattering angle $\theta_f = 5^\circ$ the angular distribution of the electrons is observed with a highest probability at the maximum values of TDCSs, which occur at the following detection angles: $\theta_e \simeq -61^\circ$ in Fig. 2(a), $\theta_e \simeq -40^\circ$ in Fig. 2(b), $\theta_e \simeq -38^\circ$ in Fig. 2(c), and $\theta_e \simeq -39^\circ$ in Fig. 2(d). Similar to free-free transitions or other laser-assisted processes [7,29,38], the net effect of the laser field is to decrease the peak values of the angular distributions of TDCSs, which is visible in Figs. 2(e)–2(h), while the atomic dressing contribution is increasing with photon energy, as illustrated in Figs. 2(a)–2(d). The dressing effect of the laser is included in the argument of the Bessel function through the quiver motion amplitude, α_0, in the electronic transition amplitudes, Eqs. (18) and (29), as well through $\mathcal{R}_q$ and the factor $\alpha_0\,\omega$ in the atomic transition amplitudes, Eqs. (20) and (31). Thus, as the photon energy increases, the atomic dressing effects (included in the full lines) are more important than the electronic dressing effects (included in the dashed lines), and the TDCS decreases as suggested by Eqs. (40), (41), and (42) derived in the low-photon en-

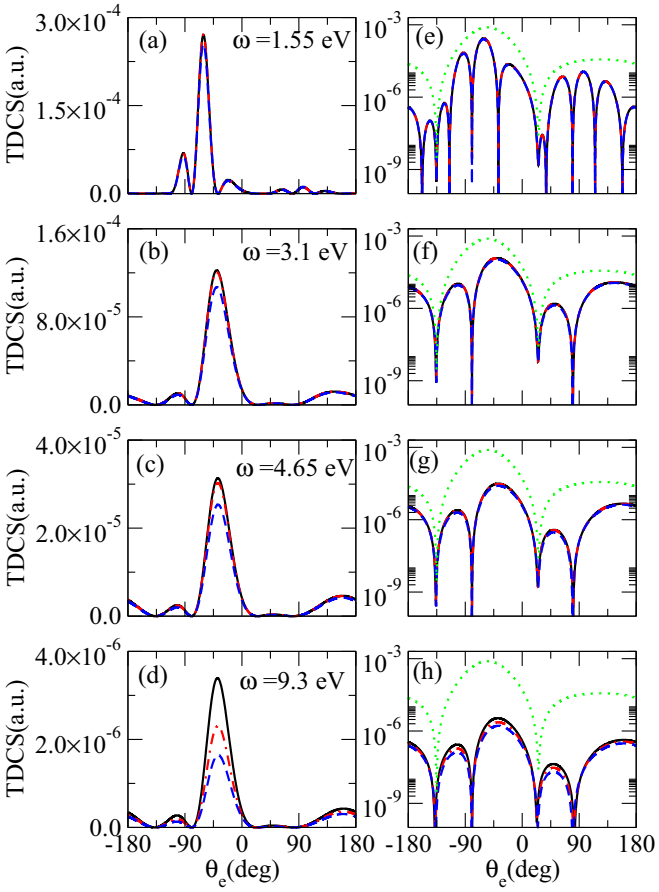

FIG. 2. The TDCSs, in atomic units, for the ionization of hydrogen from the ground state by electron impact in the presence of a LP laser field with $\boldsymbol{\varepsilon} \| \boldsymbol{k}_i$, as a function of the ejected electron angle θ_e, for one-photon absorption. The kinetic energies of the incident and ejected electron are $E_i = 2$ keV and $E_e = 200$ eV, and the scattering angle is $\theta_f = 5^\circ$. The laser intensity is $I = 1$ TW/cm^2, while the photon energy is $\omega = 1.55$ eV in Fig. 2(a), 3.1 eV in Fig. 2(b), 4.65 eV in Fig. 2(c), and 9.3 eV in Fig. 2(d). The solid lines correspond to the laser-assisted TDCSs calculated from Eq. (48), the dashed lines correspond to TDCSs in which the atomic dressing is neglected, and dot-dashed lines correspond to TDCSs in which the atomic dressing is considered in the LFA. Figures 2(e)–2(h) show the same results of the laser-assisted TDCSs as in Figs. 2(a)–2(d), but in a logarithmic scale, in which the dotted line represent the TDCS in the absence of the laser field.

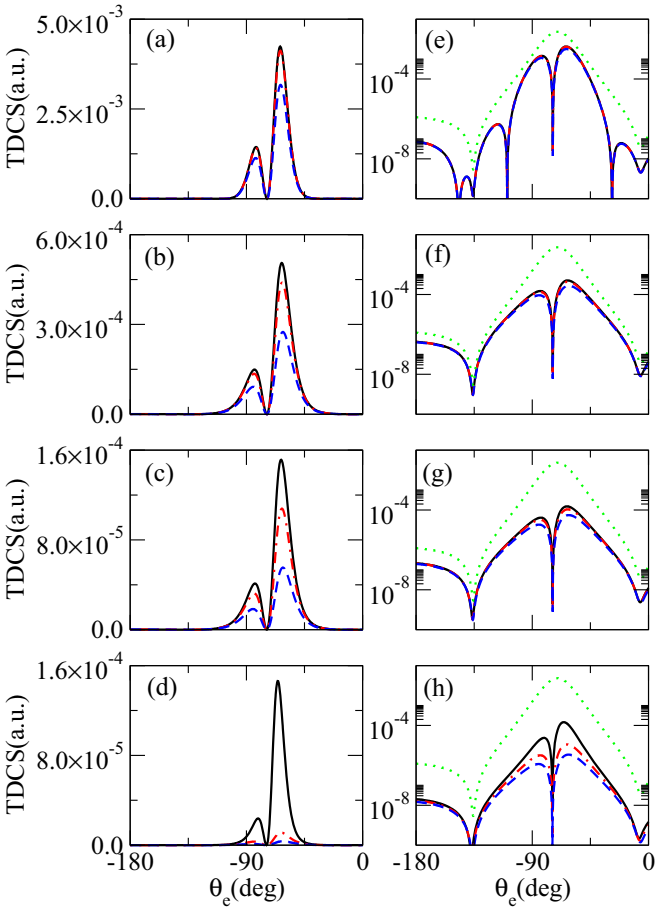

FIG. 3. Similar result as in Figs. 2(a)–2(h), but for a scattering angle $\theta_f = 15^\circ$.

ergy limit. At low photon energies which are far from any atomic resonance, of 1.55 eV or even 3.1 eV at $\theta_f = 5^\circ$, the laser-assisted $(e, 2e)$ process depicted in Figs. 2(a), 2(b), and 3(a) is well described by the LFA (dot-dashed lines), as long as the photon energy is much smaller than $|E_1|$. A clear signature of the nonperturbative effect of the laser is the oscillatory character of the angular distribution of TDCS, as shown in Fig. 2(a) compared to Figs. 2(b)–2(d). The nonperturbative behavior, due to a larger quiver amplitude, is seen at the small photon energy of 1.55 eV ($\alpha_0 \simeq 1.64$ a.u. and $U_p \simeq 0.03$ eV), and resides in the occurrence of an increasing number of zeros in the Bessel functions of the first kind and, therefore, in the TDCS [20]. Thus, kinematic minima of TDCSs appear at $\mathcal{R}_q = 0$ if the scalar product $\boldsymbol{\varepsilon} \cdot \mathbf{q} = 0$, condition that is fulfilled at ejected electron angles given by the relation $\cos\theta_e = (k_i - k_f \cos\theta_f)/k_e$. The first two kinematical minima which are located on the left and right side of the main maximum in Fig. 2(a) at the photon energy of 1.55 eV, occur at the angles $\theta_e \simeq -79^\circ$ and 80°, while the next minima of TDCS are due to the zeros of the Bessel function $J_1(\mathcal{R}_q)$ with $\mathcal{R}_q \neq 0$. At larger photon energies in Figs. 2(b)–2(d), the first two kinematical minima of the TDCSs occur at the angles $\theta_e \simeq -79^\circ$ in Figs. 2(b)–2(d), and at $\theta_e \simeq 80^\circ$ in Fig. 2(b), $\theta_e \simeq 81^\circ$ in Fig. 2(c), and $\theta_e \simeq 83^\circ$ in Fig. 2(d).

In Fig. 4, we show the numerical results for TDCSs plotted in a logarithmic scale for $N = 0$, 1 and 2, at $\omega = 3.1$ eV and the scattering angles $\theta_f = 5^\circ$ in Fig. 4(a) and $\theta_f = 15^\circ$ in Fig. 4(b), with the same parameters as in Figs. 2(b) and 3(b). The dotted lines in Figs. 4(a) and 4(b) represent the TDCSs in the absence of the laser field. The magnitude of the laser-assisted TDCS with no photon exchange ($N = 0$) is comparable to that of the field-free case because at moderate intensities the laser field does not contribute to the ionization process. The differences between the field-free and laser-assisted TDCSs at $N = 0$ are more noticeable at small scattering angles $\theta_f = 5^\circ$ in Fig. 4(a) around the main peak located at $\theta_e = -55^\circ$ and around backward scattering angles $\theta_e = \pm 180^\circ$ in both Figs. 4(a) and 4(b). For $N \neq 0$, the

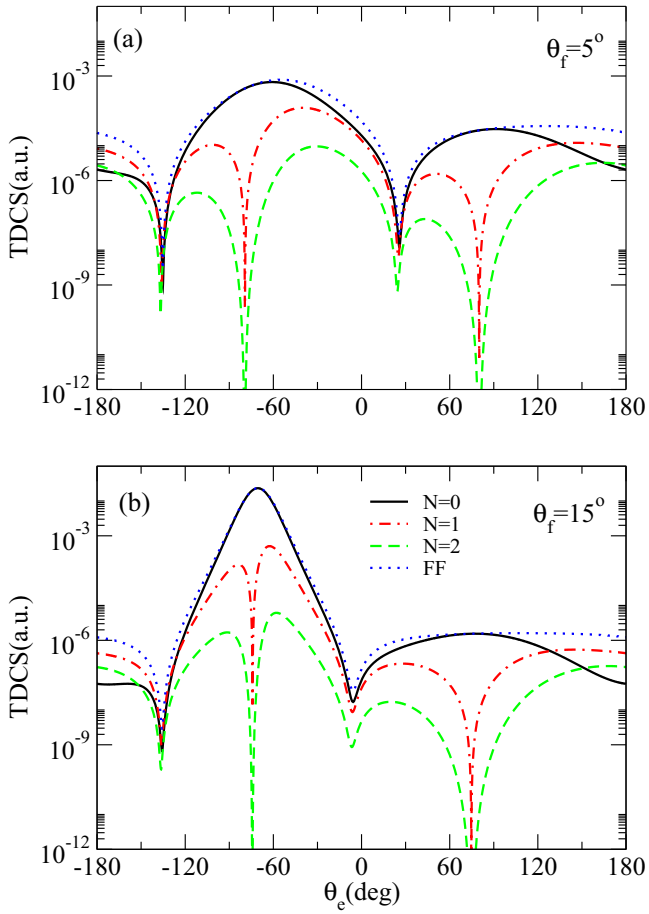

FIG. 4. The TDCSs for the ionization of hydrogen by electron impact in the presence of a LP laser field as a function of the ejected electron angle, θ_e, at the photon energy $\omega = 3.1$ eV for no photon exchange (full line) and one- and two-photon absorption (dot-dashed and dashed lines). The dotted lines represent the TDCSs in the absence of the laser field (FF). The scattering angle is $\theta_f = 5^\circ$ in Fig. 4(a) and $\theta_f = 15^\circ$ in Fig. 4(b). The other parameters concerning the scattering geometry, incident and ejected electron energies, and laser intensity are the same as in Fig. 2.

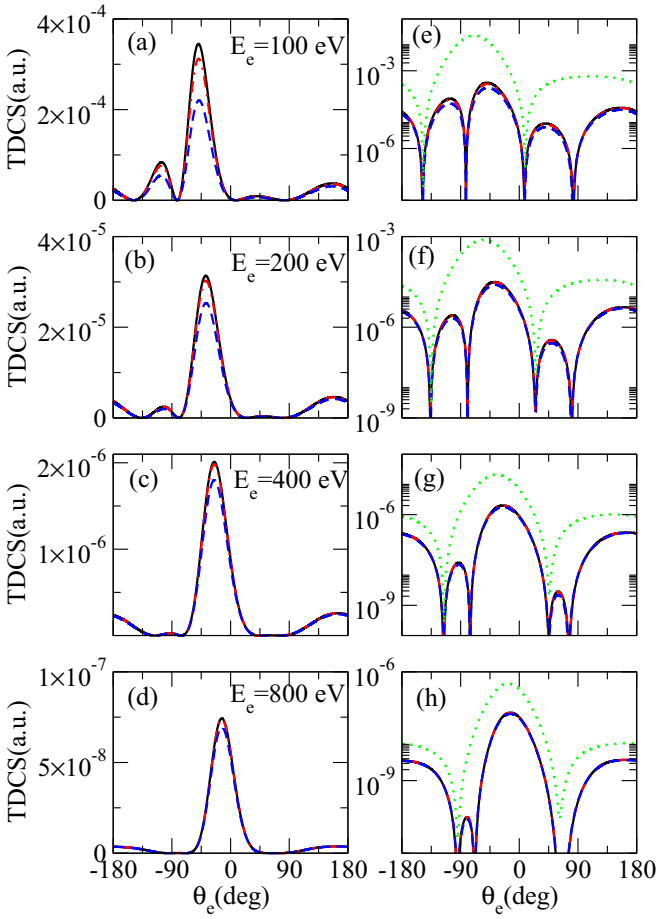

FIG. 5. The TDCSs for the ionization of hydrogen by electron impact in the presence of a LP laser field as a function of the ejected electron angle θ_e, for one-photon absorption. The photon energy is $\omega = 4.65$ eV, while the kinetic energy of the ejected electron is $E_e = 100$ eV in Fig. 5(a), 200 eV in Fig. 5(b), 400 eV in Fig. 5(c), and 800 eV in Fig. 5(d). The other parameters concerning the scattering geometry, kinetic energy of the incident projectile, angle of the scattered electron, and laser intensity are the same as in Fig. 2. Figures 5(e)–5(h) show the same results of the laser-assisted TDCSs as in Fig. 5(a)–5(d), but in a logarithmic scale. The dotted lines in Figs. 5(e)–5(h) represent the TDCSs in the absence of the laser field.

magnitude of the TDCS main peak is significantly smaller than that of the field-free case. The angular distributions of TDCS at different N present similar features with different magnitudes and show that the net effect of the laser field is to decrease the values of TDCSs and to split the peaks which occur at $N = 0$ (full lines) at $\theta_e \simeq -62^\circ$ in Fig. 4(a) and $\theta_e \simeq -71^\circ$ in Fig. 4(b). The splitting of the peaks by the kinematical minima, which is a well-known signature of the laser field on the TDCSs, appears due to cancellation of the scalar product $\boldsymbol{\varepsilon} \cdot \mathbf{q}$ and is located almost symmetrically with respect to the direction of the incident electron at the ejected angles $\theta_e \simeq -79^\circ$ and 80° in Fig. 4(a) and $\theta_e \simeq -74^\circ$ and 75° in Fig. 4(b).

It is well known that the projectile electron plays a major role in the scattering process since it interacts with the atomic target electron (a repulsive interaction), its nucleus (an attractive interaction), and the laser field. In what follows, we want to discuss the role of the fast ejected electron in the laser-assisted $(e, 2e)$ ionizing collisions. In Fig. 5, we present the TDCSs for the ionization of hydrogen by electron impact in the presence of a LP laser field, for absorption of one photon $N = 1$, at a photon energy of 4.65 eV as a function of the ejected electron angle. The kinetic energy of the ejected electron is $E_e = 100$ eV in Fig. 5(a), 200 eV in Fig. 5(b), 400 eV in Fig. 5(c), and 800 eV in Fig. 5(d). The other parameters concerning the scattering geometry, incident projectile energy, angle of the scattered electron, and laser field intensity are the same as in Fig. 2. Figures 5(e)–5(h) illustrate, in a logarithmic scale, the same results of the laser-assisted TDCSs as in Figs. 5(a)–5(d) together with the field-free TDCSs, which are represented by the dotted lines. Figure 6 shows similar results as in Fig. 5, but for a larger scattering angle $\theta_f = 15^\circ$. Clearly, the electronic contribution (dashed lines) underestimates the angular distribution of TDCS. For kinetic

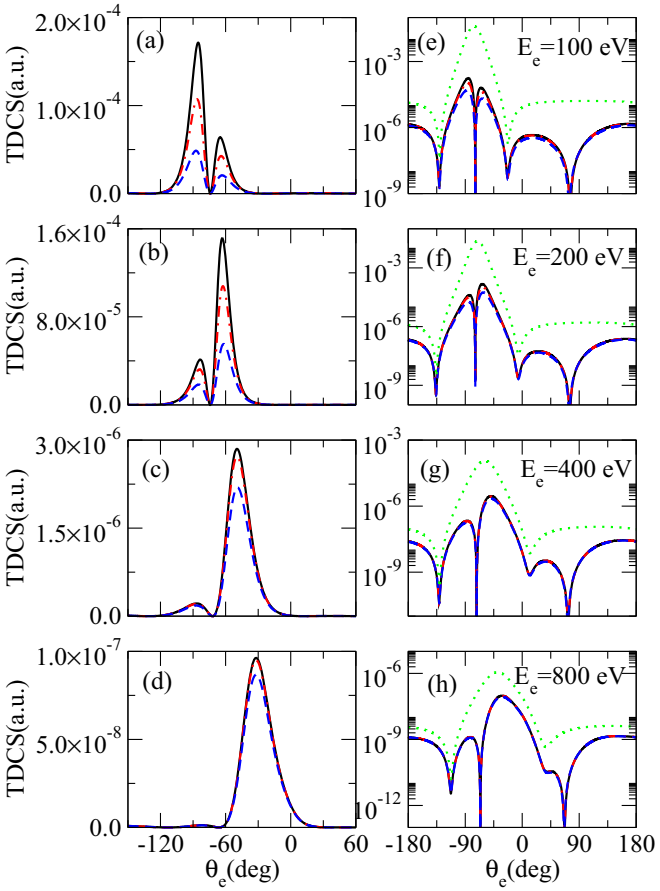

FIG. 6. Similar result as in Figs. 5(a)–5(h), but for a scattering angle $\theta_f = 15^\circ$.

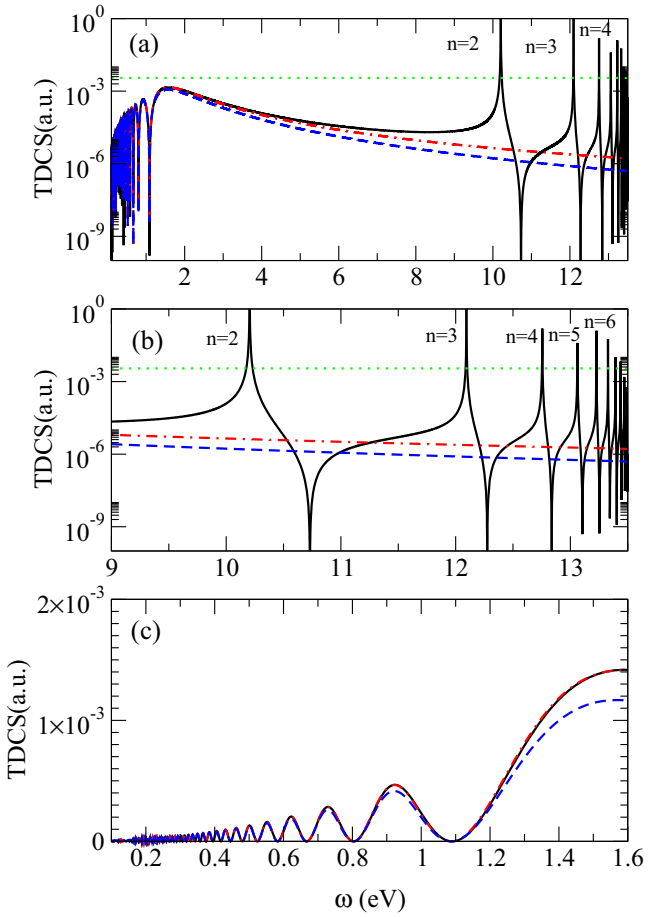

FIG. 7. The TDCSs for the ionization of hydrogen by electron impact in the presence of a LP laser field as a function of the photon energy ω, for one-photon absorption. The solid lines correspond to the laser-assisted TDCSs calculated from Eq. (48), the dashed lines correspond to TDCSs in which the atomic dressing is neglected, and dot-dashed lines correspond to TDCSs in which the atomic dressing is considered in the LFA. The angles of the scattered and ejected electrons are $\theta_f = 15^\circ$ and $\theta_e = -55^\circ$, while the incident and ejected electron kinetic energies, and laser intensity are the same as in Fig. 2. Figure 7(b) shows the detailed structure of the resonance peaks which occur at photon energies $\omega = |E_1|(1 - 1/n^2)$, with $n \geqslant 2$. Figure 7(c) shows, in a linear scale, the detailed structure of the oscillatory behavior of TDCS at small photon energies, $\omega \leqslant 1.6$ eV.

energies of the ejected electron $E_e \leqslant 100$ eV at $\theta_f = 5^\circ$ and $E_e \leqslant 200$ eV at $\theta_f = 15^\circ$, the atomic dressing effects are quite important, and the TDCS calculated in the LFA (dot-dashed lines) fails to describe accurately the laser-assisted $(e, 2e)$ process. As the kinetic energy of the ejected electron increases to 800 eV, at small scattering angles the atomic dressing effects are less important than the electronic dressing effects, as shown in Figs. 5(d) and 6(d). As we approach the symmetric coplanar case of scattered and ejected electrons of equal energies, $E_f \simeq E_e \simeq (E_i + E_1 + \omega)/2$, the minimum of the recoil momentum amplitude q occurs now at larger angles close to $\theta_f \simeq -\theta_e \simeq 45^\circ$, Eq. (54).

In order clarify the importance of the atomic dressing term, we illustrate in Fig. 7(a) the TDCS, in a logarithmic scale, with respect to the photon energy for one-photon absorption. The kinetic energies of the projectile and the ejected electrons are $E_i = 2$ keV and $E_e = 200$ eV, while the angles of the scattered and ejected electrons are chosen $\theta_f = 15^\circ$ and $\theta_e = -55^\circ$. The motivation of choosing the ejected electron angle $\theta_e = -55^\circ$ is related to position of the mean peak of the field-free TDCS in Fig. 2(e), which occurs at the minimum value of the recoil momentum q. The polarization vector of the electric field is parallel to the momentum of the incident electron, and we consider a moderate laser intensity, $I = 1$ TW/cm^2, for which the nonperturbative dressing effects of the projectile and ejected electrons can be visualized at small photon energies with $\alpha_0 > 1$. The solid line corresponds to the laser-assisted TDCS calculated from Eq. (48), which includes the dressing effects of the projectile and of the atomic target, the dashed line corresponds to TDCS in which the atomic dressing terms are neglected, while the dot-dashed line corresponds to the result in which the atomic dressing terms are considered in the LFA, Eq. (38). The TDCS shows a strongly dependence on the atomic structure of the target and exhibits a series of resonance peaks which are associated with one-photon absorption from the initial ground state of the hydrogen atom, at photon energies that match atomic resonances $\omega = E_n - E_1$, and correspond to poles that occur in the atomic radial integral at $\tau = n$, with $n \geqslant 2$, as detailed in Fig. 7(b). The noteworthy feature of the atomic radial integral J_{101}, Eq. (25), is that it presents poles with

respect to τ which arise due to the cancellation of the $2-\tau$ factor in the denominator, as well as from the poles of the Appell's hypergeometric functions F_1 at $\tau = n'$, where $n' \geqslant 3$ is an integer. The origin of these poles resides in the poles of the Coulomb Green's functions used for the calculation of the linear-response vector $\mathbf{w}_{100}$ [34]. Because our perturbative approach of the laser-atom interaction neglects the widths and radiative shifts of the atomic levels, a two-level atom would be suitable at photon energies that match atomic resonances in order to evaluate TDCS. Nevertheless, our theoretical model provides useful information regarding the qualitative behavior of the TDCS in the vicinity of resonances. Clearly, the LFA, which does not take into account the atomic structure, fails to describe the laser-assisted $(e, 2e)$ process at large photon energies (typically in the UV range). Figure 7(c) shows the energy spectra in the nonperturbative regime at low photon energies, $\omega \leqslant 1.6$ eV in Fig. 7(a), domain where at the laser intensity $I = 1$ TW/cm^2 the quiver amplitude α_0 is larger than 1 a.u. and increases up to 395 a.u. for $\omega = 0.1$ eV. The TDCS presents oscillations due to the Bessel function $J_1(\mathcal{R}_q)$, and the LFA (dot-dashed line) gives a good description of the atomic dressing effect. It should be kept in mind that both the laser intensity and photon energy play an important role, and obviously, the nonperturbative effects are seen to be important as laser intensity increases and photon energy decreases due to increasing quiver motion of the free and bound electrons, and contribute to the oscillatory behavior of the laser-assisted TDCSs, which resides in the occurrence of increasing oscillations of the Bessel function.

In the end, we want to examine the exchange effects between the ejected and scattered electrons by comparing the direct and exchange contributions to TDCS. Thus, in Fig. 8 we display the TDCS for the ionization of hydrogen by electron impact in the presence of a LP laser field as a function of the kinetic energy of the ejected electron, E_e, for one-photon absorption at $\omega = 4.65$ eV. The solid lines represent the total laser-assisted TDCSs calculated from Eq. (48), the dot-dashed lines correspond to TDCSs for the direct channel with the exchange contributions neglected in Eq. (48), and the dashed lines correspond to TDCSs for the exchange channel with the direct contributions neglected in Eq. (48). We present the numerical results for three fixed scattering angles, θ_f, namely 0° in Figs. 8(a) and 8(d), 5° in Figs. 8(b) and 8(e), and 15° in Figs. 8(c) and 8(f), while the angles of the ejected electron, θ_e, are considered 5° and −55° in the left- and right-hand panels, respectively. The kinetic energy of the incident electron is 2 keV and laser intensity is 1 TW/cm^2. We should underline the main difference between the electronic and atomic transition amplitudes of the direct scattering channel, Eqs. (19) and (23), which vary like Δ^{-2} and those corresponding to the exchange scattering channel, Eqs. (30) and (33), which vary like Δ_e^{-2}, as shown in Subsecs. II B and II C. We note that the exchange terms cannot be neglected in comparison to the contribution of the direct scattering channel to TDCS, if the momentum transfer of the ejected electron Δ_e is comparable with Δ or lower. Obviously, the former case occurs in the particular case of symmetric kinematics with $E_e = E_f$ and $\theta_e = \theta_f$, as happens in the EMS experiments, in which the momentum

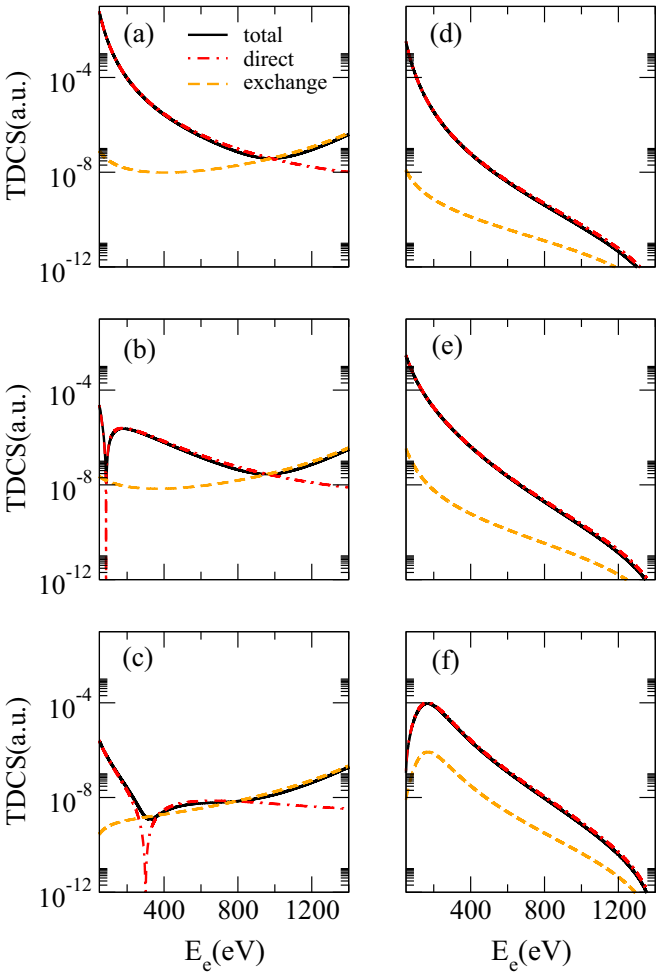

FIG. 8. The TDCSs for the ionization of hydrogen by electron impact in the presence of a LP laser field as a function of the kinetic energy of the ejected electron E_e, for one-photon absorption. The solid lines represent the total laser-assisted TDCSs calculated from Eq. (48), the dot-dashed lines correspond to TDCSs in which the exchange contribution is neglected (direct TDCSs), and the dashed lines correspond to TDCSs in which the direct contribution is neglected (exchange TDCSs). The angles of the scattered and ejected electrons are $\theta_f = 0°$ in Figs. 8(a) and 8(d), 5° in Figs. 8(b) and 8(e), and 15° in Figs. 8(c) and 8(f), while $\theta_e = 5°$ and $-55°$ in the left- and right-hand panels, respectively. The rest of the parameters, incident electron energy, photon energy, and laser intensity, are the same as in Fig. 5.

transfers become equal $\Delta_e = \Delta$ and take minimum values at forward scattering. At a small ejected angle of $\theta_e = 5°$ in Figs. 8(a)–8(c) it is quite clear that the TDCS for the exchange channel become larger in comparison to the direct channel for kinetic energies of the ejected electron corresponding to $\Delta_e < \Delta$, i.e., at kinetic energies E_e larger than 980 eV in Fig. 8(a), 960 eV in Fig. 8(b), and 790 eV in Fig. 8(c), while at a larger ejected angle of $\theta_e = -55°$ in Figs. 8(d)–8(f) the exchange terms can be neglected since $\Delta_e > \Delta$. Further, we plot in Figs. 9(a)–9(c) the dependence of the total (full lines), direct (dot-dashed lines), and exchange (dotted lines) TDCSs on the laser photon energy at three kinetic energy of the ejected electron of $E_e = 200$ eV in Fig. 9(a), 600 eV in Fig. 9(b), and

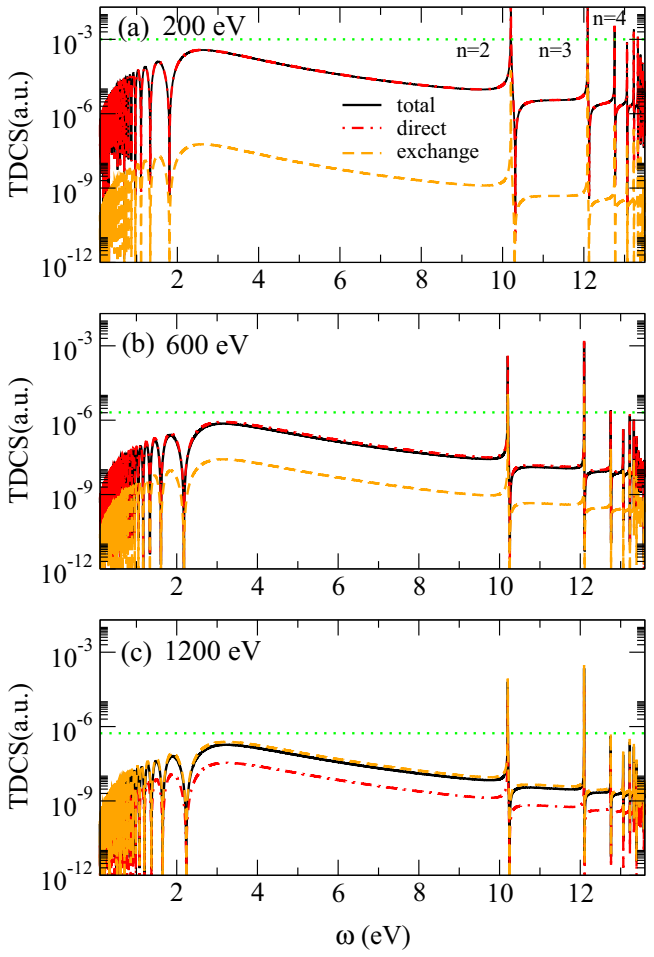

FIG. 9. The TDCSs for the ionization of hydrogen by electron impact in the presence of a LP laser field as a function of the photon energy ω, for one-photon absorption. The solid lines correspond to the total laser-assisted TDCSs calculated from Eq. (48), the dot-dashed lines correspond to TDCSs in which the exchange contribution is neglected (direct TDCSs), and the dashed lines correspond to TDCSs in which the direct contribution is neglected (exchange TDCSs). The dotted lines represent the TDCSs in the absence of the laser field. The kinetic energy of the ejected electron is $E_e = 200$ eV in Fig. 9(a), 600 eV in Fig. 9(b), and 1200 eV in Fig. 9(c). The angles of the ejected and scattered electrons are $\theta_e = 5^\circ$ and $\theta_f = 0^\circ$, while the kinetic energy of the incident electron and laser intensity are the same as in Fig. 8.

1200 eV in Fig. 9(c), for the ejected and scattering angles $\theta_e = 5^\circ$ and $\theta_e = 0^\circ$. The kinetic energy of the incident electron and laser intensity are the same as in Fig. 8, and the dotted lines represent the TDCSs in the absence of the laser field. At $E_e = 1200$ eV the exchange effects dominates over direct scattering process in contrast to TDCS at lower kinetic energies of the ejected electron plotted in Figs. 9(a) and 9(b). Therefore at small scattering and ejected angles for large kinetic energy of the ejected electron such that $\Delta_e < \Delta$ the exchange contributions to TDCS can become larger than the direct ones and dominates the spectral distribution. The final comment that we make here is that as long when the momentum transfer Δ is smaller than Δ_e we can safely neglect the exchange effects.

IV. SUMMARY AND CONCLUSIONS

We study the electron-impact ionization of hydrogen at large projectile and ejected electron kinetic energies in the presence of a linearly polarized laser field and investigate the laser-assisted $(e, 2e)$ reaction at moderate laser field intensities. We focus our numerical results on the case of the asymmetric coplanar scattering geometry, where we discuss the importance of the dressing effects and analyze the influence of the laser field on the TDCS in several numerical examples. The laser-assisted $(e, 2e)$ reaction has a nonlinear character which consists in multiphoton absorption (emission) of photons from (to) laser radiation by projectile and ejected electrons and atomic target. We present a method to calculate the atomic radial amplitude in a closed form, which represents the main difficulty in the evaluation of TDCS. Thus, a semiperturbative approach is used, in which for the interaction of the fast incident and outgoing electrons with the laser field we employ nonperturbative Gordon-Volkov wave functions, while the interaction of the hydrogen atom with the laser field is considered in first-order TDPT, and the interaction of the fast incident electron with the hydrogen atom is treated in the first-order Born approximation. The exchange between the outgoing electrons cannot be ignored when ejected electrons with large kinetic energy are detected, and is included in the calculation. Our theoretical formulas and numerical results clearly demonstrate the strong influence of the photon energy and laser intensity on the dynamics of laser-assisted $(e, 2e)$ process.

It was found that the atomic dressing contribution calculated in first-order TDPT in the laser field substantially modifies the laser-assisted TDCSs at small momenta q, Δ, and Δ_e, and for photon energies close to resonances. The introduction of the laser field in the $(e, 2e)$ reaction changes the profile of TDCS as it is seen in Fig. 4, where the peaks of TDCSs are reduced in magnitude and split by the presence of the laser, due to appearance of the kinematical minima. We show that the atomic dressing effects strongly depend on the structure of the atomic target and cannot be correctly described by the LFA at large photon energies. At low photon energies, we confirm the validity of LFA by comparing the numerical results obtained for the atomic matrix elements within LFA with the results obtained by first-order TDPT. For slow ejected electrons, $E_e \ll E_f$, we can safely neglect the exchange effects as long as the momentum transfer Δ is smaller than Δ_e.

Thus, the theoretical studies remain very useful for understanding essential details of the scattering signal due to the fact that the derived analytical formulas have the advantage of giving more physical insight into the laser-assisted $(e, 2e)$ process and valuable information in future theoretical and experimental investigations.

ACKNOWLEDGMENTS

This work was supported by the Romanian Ministry of Research, Innovation, and Digitization, Grant No. 16N/2019, within the National Nucleus Program.

[1] F. W. Byron, Jr. and C. J. Joachain, Phys. Rep. **179**, 211 (1989).

[2] C. T. Whelan, H. R. J. Walters, A. Lahmam-Bennani, and H. Ehrhardt, editors, *(e, 2e) and Related Process*, NATO ASI Series (Springer, Dordrecht, 1993) Vol. 414; C. T. Whelan and H. R. J. Walters, *editors, Coincidence Studies of Electron and Photon Impact Ionization* (Springer Science+Business Media, New York, 1997).

[3] R. Camilloni, A. Giardini Guidoni, R. Tiribelli, and G. Stefani, Phys. Rev. Lett. **29**, 618 (1972).

[4] E. Weigold and I. E. McCarthy, *Electron Momentum Spectroscopy* (Kluwer, New York, 1999).

[5] V. G. Neudachin, Y. V. Popov, and Y. F. Smirnov, Phys. Usp. **42**, 1017 (1999).

[6] M. A. Coplan, J. H. Moore, and J. P. Doering, Rev. Mod. Phys. **66**, 985 (1994).

[7] F. Ehlotzky, A. Jaroń, and J. Z. Kamiński, Phys. Rep. **297**, 63 (1998).

[8] C. Höhr, A. Dorn, B. Najjari, D. Fischer, C. D. Schröter, and J. Ullrich, Phys. Rev. Lett. **94**, 153201 (2005); J. Electron Spectrosc. Relat. Phenom. **161**, 172 (2007).

[9] T. Hiroi, Y. Morimoto, R. Kanya, and K. Yamanouchi, Phys. Rev. A **104**, 062812 (2021).

[10] P. Cavaliere, G. Ferrante, and C. Leone, J. Phys. B **13**, 4495 (1980); P. Cavaliere, C. Leone, R. Zangara, and G. Ferrante, Phys. Rev. A **24**, 910 (1981).

[11] M. Jain and N. Tzoar, Phys. Rev. A **18**, 538 (1978).

[12] J. Banerji and M. H. Mittleman, J. Phys. B **14**, 3717 (1981).

[13] V. Gordon, Z. Phys. **40**, 117 (1926).

[14] D. M. Wolkow, Z. Phys. **94**, 250 (1935).

[15] C. J. Joachain, P. Francken, A. Maquet, P. Martin, and V. Véniard, Phys. Rev. Lett. **61**, 165 (1988).

[16] F. W. Byron,, Jr. and C. J. Joachain, J. Phys. B **17**, L295 (1984).

[17] H. Ehrhardt, K. Jung, G. Knoth, and P. Schlemmer, Z. Phys. D: At. Mol. Clusters **1**, 3 (1986).

[18] P. Martin, V. Véniard, A. Maquet, P. Francken, and C. J. Joachain, Phys. Rev. A **39**, 6178 (1989).

[19] R. Taïeb, V. Véniard, A. Maquet, S. Vučić, and R. M. Potvliege, J. Phys. B: At. Mol. Opt. Phys. **24**, 3229 (1991).

[20] A. Cionga, V. Florescu, A. Maquet, and R. Taïeb, Phys. Rev. A **47**, 1830 (1993).

[21] A. Makhoute, D. Khalil, and I. Ajana, Atoms **7**, 40 (2019).

[22] K. A. Kouzakov, Y. V. Popov, and M. Takahashi, Phys. Rev. A **82**, 023410 (2010).

[23] A. A. Bulychev, K. A. Kouzakov, and Y. V. Popov, Phys. Lett. A **376**, 484 (2012).

[24] D. Khalil, M. Tlidi, A. Makhoute, and I. Ajana, J. Phys. B: At. Mol. Opt. Phys. **50**, 078001 (2017).

[25] L. V. Keldysh, Sov. Phys. JETP **20**, 1307 (1965).

[26] F. H. M. Faisal, J. Phys. B: At. Mol. Phys. **6**, L89 (1973).

[27] H. R. Reiss, Phys. Rev. A **22**, 1786 (1980).

[28] B. H. Bransden and C. J. Joachain, *Physics of Atoms and Molecules* (Longman, London, 1983).

[29] C. J. Joachain, N. J. Kylstra, and R. M. Potvliege, *Atoms in Intense Laser Fields* (Cambridge University Press, Cambridge, UK, 2012), p. 466.

[30] B. Lohmann and E. Weigold, Phys. Lett. A **86**, 139 (1981).

[31] C. Leone, S. Bivona, R. Burlon, F. Morales, and G. Ferrante, Phys. Rev. A **40**, 1828 (1989).

[32] Y. Attaourti and S. Taj, Phys. Rev. A **69**, 063411 (2004).

[33] J. Zhang and T. Nakajima, Phys. Rev. A **75**, 043403 (2007).

[34] V. Florescu and T. Marian, Phys. Rev. A **34**, 4641 (1986).

[35] A. Cionga, F. Ehlotzky, and G. Zloh, Phys. Rev. A **62**, 063406 (2000); J. Phys. B: At. Mol. Opt. Phys. **33**, 4939 (2000).

[36] G. Buica, Phys. Rev. A **92**, 033421 (2015); G. Buică, J. Quant. Spectrosc. Radiat. Transfer **187**, 190 (2017).

[37] A. Cionga, F. Ehlotzky, and G. Zloh, Phys. Rev. A **61**, 063417 (2000).

[38] A. Cionga and G. Zloh, Laser Phys. **9**, 69 (1999).

[39] A. Dubois and A. Maquet, Phys. Rev. A **40**, 4288 (1989).

[40] N. F. Mott and H. S. W. Massey, *The Theory of Atomic Collisions* (Oxford University Press, London, 1965); C. Joachain, Quantum Collision Theory (North-Holland, Amsterdam, 1987).

[41] G. N. Watson, *Theory of Bessel Functions* (Cambridge University Press, Cambridge, UK, 1962).

[42] E. Weigold, C. J. Noble, S. T. Hood, and I. Fuss, J. Phys. B: At. Mol. Phys. **12**, 291 (1979).

[43] A. Dubois, A. Maquet, and S. Jetzke, Phys. Rev. A **34**, 1888 (1986).

[44] V. I. Ochkur, Sov. Phys. JETP **20**, 1175 (1965).

[45] M. Jauch and F. Rohrlich, *The Theory of Electrons and Photons* (Springer, New York, 1976).

[46] F. E. Low, Phys. Rev. **110**, 974 (1958).

[47] Y. Miyake, M. Takahashi, N. Watanabe, Y. Khajuria, Y. Udagawa, Y. Sakai, and T. Mukoyama, Phys. Chem. Chem. Phys. **8**, 3022 (2006).

[48] N. M. Kroll and K. M. Watson, Phys. Rev. A **8**, 804 (1973).